Student thesis series INES nr 432

Watershed delineation for runoff estimations to culverts in the Swedish road network
- A comparison between two GIS based hydrological modelling methods and a manually delineated watershed

Iris Behrens

2017
Department of
Physical Geography and Ecosystem Science
Lund University
Sölvegatan 12
S-223 62 Lund
Sweden

Iris Behrens (2017)

Watershed delineation for runoff estimations to culverts in the Swedish road network – A comparison between two GIS based hydrological modelling methods and a manually delineated watershed

Avgränsning av avrinningsområden för uppskattning av vattenflöden till kulvertar i det svenska vägnätet – En jämförelse mellan två GIS baserade hydrologiska modeller och ett manuellt inmätt avrinningsområde

Master degree thesis, 30 credits in Geomatics
Department of Physical Geography and Ecosystem Science, Lund University

Level: Master of Science (MSc)

Course duration: January 2017 until June 2017

Watershed delineation for runoff estimations to culverts in the Swedish road network – A comparison between two GIS based hydrological modelling methods and a manually delineated watershed

---

Iris Behrens

Master thesis, 30 credits, in Geomatics

Supervisor
Andreas Persson
Department of Physical Geography and Ecosystem Science

Exam committee:

Micael Runnström
Department of Physical Geography and Ecosystem Science

Petter Pilesjö
Department of Physical Geography and Ecosystem Science

Abstract

The anticipated climate changes are predicted to alter the precipitation patterns in Sweden. Increased episodes of intense short-duration rainfall and higher intensities of day long-duration rainfall are expected. Road sections are often a target of flooding, causing impassable roads, due to the lack of capacity of drainage systems. One of the factors determining the water flow to a depression is the size of the contributing watershed. In this study, catchments derived from two flow routing methods, the deterministic eight-node algorithm (D8) and the Triangular Form-based Multiple flow algorithm (TFM), are compared to a manually measured watershed, to investigate the runoff to a single culvert. For further comparison of the modelled catchments the elevation of the data is modified into different height intervals. The deviations between the modelled catchments to the manually delineated watershed are noticeable regarding both size and shape. The differences between the modelled watersheds are minor concerning size, shape and location. Based on the six digital elevation models tested in this study, the TFM catchments covered a greater area in comparison to the D8 catchments when the vertical resolution is high, whilst the D8 watersheds cover a greater area when the vertical resolution is low. According to the estimated 50-, 100- and 200-year flows, the investigated culvert is not likely to be flooded.

Keywords

GIS, Hydrological modelling, Watershed, Single flow direction algorithm, Multiple flow direction algorithm, Climate change adaption

Populärvetenskaplig sammanfattning

Till följd av de förväntade klimatförändringarna beräknas nederbördsmönstren i Sverige att förändras. Episoder av intensiv och kortvarig nederbörd förväntas öka på flertal ställen i landet, samt att utsträckningen av långvarig nederbörd, som kan pågå under flera dagar, även den, förväntas att öka. Det svenska vägnätet stöter redan idag på problem att möta de förändrade nederbördsmängderna, då vägsektioner är ofta blir ett mål för översvämning. Ansamlingar av regn vid låga punkter längst vägarna, orsakar blockerade och översvämmade vägar, vilket ofta är ett resultat av brist på kapacitet i våra befintliga dräneringssystem.

En av de faktorer som kan användas då man bestämmer vattenflödet till en sänka längst vägen, är storleken på avrinningsområdet som bidrar med vatten till denna punkt. Avrinningsområden kan mätas upp manuellt, men idag är det vanligt att avrinningsområden avgränsas digitalt med hjälp av höjddata i GIS-miljö. För att avgöra avgränsningen av det område som bidrar med avrinning till en punk digitalt, finns det flertal flödesriktningsalgoritmer att välja mellan. I denna studie jämförs avrinningar från två flödesriktningsalgoritmer, den Deterministiska åtta nodalgoritmen (D8) och den Triangulära formbaserade multipla flödesriktnings-algoritmen (TFM), med ett manuellt uppmätt avrinningsområde. Genom att använda arean av avrinningsområdena, kan avrinningen för olika återkomst perioder till en kulvert undersökas. För ytterligare jämförelse av de storleken på de modellerade avrinningsområdena modifierades även höjddata till lägre upplösningar. Skillnaderna mellan de modellerade avrinningsområdena till den manuellt avgränsade avrinningsområdet är märkbara med avseende på både storlek och form. Skillnaderna mellan de modellerade avrinningsområdena är små, då storleken, formen och plats är snarlika. Baserat på de sex digitala höjdmodellerna som testades i denna studie täckte avrinningsområdena generade av TFM modellen ett större område i jämförelse med D8-avrinningsområdena när den vertikala upplösningen är hög. Avrinningsområdena skapade av D8 modellen täcker dock ett större område när den vertikala upplösningen är låg, jämfört med de avrinningsområdena genererade av TFM modellen.

Nyckelord
GIS, Hydrologisk modellering, Avrinningsområde, flödesriktningsalgoritm, Klimatanpassning

Table of content

Abbreviations

D8	Deterministic eight-node algorithm
DEM	Digital Elevation Model
GIS	Geographical Information System
MFD	Multiple Flow Direction
SFD	Single Flow Direction
TFM	Triangular Form-based multiple Flow algorithm
TIN	Triangular Irregular Network

Acknowledgements

First and foremost, I like to thank my supervisor Andreas Persson for your ideas and support throughout the semester. Secondly, I like to thank Jenny Rassmus and Agne Gunnarsson at Trafikverket for your input, suggestions and supplying me with data. In addition, I would like to thank the city planning office at Växsjö municipality for supplying me additional data and information about the culvert. Also, a big thanks to John Bengtsson for your encouragements.

1. Introduction

The evidences of climate change are becoming further amplified by the Intergovernmental Panel on Climate Change (Meyer et al., 2014). Climate, which in simple terms, can be described as the average day-to-day weather during a certain period of time. The mean of variables such as precipitation and temperature, are commonly measured over a 30-year period. As for the latest measured periods, temperatures hit its warmest since the last 1400 years in the Northern Hemisphere. Since hydrological processes are mainly driven by climate, further alterations in global, regional and local hydrological systems can be expected. Variations in precipitation and snow melting are already observed in many regions, causing the hydrological systems to change (Allen et al., 2013).

Anticipated changes in the atmospheric composition would redistribute the precipitation patterns in parts of Sweden, meaning more frequent episodes of intense short-duration rainfall and higher intensities of day long-duration rainfall (Olsson & Foster, 2013). Also, increased temperatures would cause significant changes in components of the surface hydrology systems, altering the levels of soil moisture, vegetation periods, snow melting etc. (Olsson et al., 2016). According to Christensen & Christensen (2003) such changes can cause severe cases of flooding particularly in the northern parts of Europe. In 2007, the European Union (EU) established new directives (2007/60/EG) regarding the management of potential flooding in the coming century. Following the EU directives, the Swedish government addressed the issue by implementing a regulation 'Förordning (SFS 2009:956) om översvämningsrisker' in 2009 (Riksdagen, 2009).

The majority of flooding events in Sweden are caused by periods of prolonged rain and snow melting, and are commonly located along lakes and riversides. Flooding caused by episodes of intense precipitation generally affect limited geographical areas, but often results in greater damages (MSB, 2010). According to the Swedish government's official investigations (SOU 60:2007) local torrential rainfall, often occurring during the months of summer, is increasing throughout the country. For an instance, parts of Scania experienced high levels of flooding due to an extreme episode of precipitation in august 2014 (Svenskt Vatten, 2016).

Infrastructure is generally vulnerable to short events of high precipitation levels, due to the presence of impervious surfaces (Olsson et al., 2016). Rainfall extremes have a significant impact on urban drainage systems and can cause pluvial flooding (Barros et al., 2014). Due to the flat surfaces with low levels of infiltration, road sections are often a target of flooding, especially when submerged (Svenskt Vatten, 2016). However, infrastructure alterations take time to complete. Therefore, existing bridges, culverts and embankments will experience the higher charges of water runoff in the near future (Klimatanpassningportalen, 2016).

The Transportation Administration maintains about 45% of the roads and 85% of the railroad networks in Sweden. The management costs of the extensive network are approximated to 15 billion Swedish crowns per year. The maintenance, including damages due to seasonal events, constitutes about three quarters of the total amount (Trafikverket, 2016a). In 2014, the Transport Administration formed a strategy to face future complications arising with the predicted climate changes. The aim is to decrease, adapt and prevent infrastructural damages as a consequence of increased precipitation and extreme events. Today parts of the network struggles to manage high precipitation levels. The extent of the network complicates a comprehensive network adaption. Possible infrastructural reconstructions need to be prioritized at high-risk zones, such as submerged intersections, bridges and road culverts. By carrying through risk assessments consisting of a road and railroad data combined with precipitation and elevation data, the risk of flooding can be analysed (Trafikverket, 2016b).

Elevation data is a useful tool when modelling planetary surfaces in geographic information system (GIS) environments. A digital elevation model (DEM) is the common method to digitally represent and store elevation data, where each cell represents the corresponding elevation of the surface of a geographic location. A DEM can be structured in multiple ways, for example as a triangular irregular network (TIN) or as a regular square grid. In the later example, the elevation is stored in a matrix of rows and columns of the regularly spaced square cells (O'Callaghan and Mark, 1984; Moore et al., 1991).

With improved technology, the availability of DEMs with high spatial resolution increases. Since 2009 Lantmäteriet has been using laser scanning to collect high accuracy national elevation models for the Swedish government to supply the need of data for climate adaption (Lantmäteriet, 2016a). The technique is known as light detection and ranging (LiDAR) producing a grid of regularly spaced elevation points. Using LiDAR, small changes can be detected in the terrain and high resolution DEMs can be derived by interpolating the points. The DEM produced by LiDAR scanning, can be resampled to lower resolutions depending on the purpose of the data (Bater & Coops, 2007; Li & Wong, 2009).

The resolution of the topographic dataset is mainly affected by the sampling of the source and the interpolation techniques (Bater and Coops, 2009; Aguilar et al., 2010; Saksena and Merwade, 2015). The vertical accuracy associated with LiDAR data differ significantly compared to older DEMs derived from photogrammetry, interferometry and radar imaging. Today, high resolution LiDAR datasets with vertical resolution below the sub-metre are becoming available along with improving techniques (Aguilar et al., 2010 & Li and Wong, 2010). Increased resolution will simultaneously increase the size of the data, and the vast amount of data in LiDAR datasets affect the computational time. Also, obtaining LiDAR data is an issue of costs. Because of the practical advantages of DEMs with coarser resolution, they are still widely used today.

The application field for DEMs are wide and there are numerous algorithms for extracting topographical, geomorphic and hydrologic information. One of the main challenges faced in hydrological modelling today, is determining the directions of the flow through the landscape.

Hydrological characteristics such as ridgelines, channel networks, catchments, sub-catchments etc. are some of the features that can be derived through elevation flow routing (Moore et al., 1991; Li & Wong, 2009; Wilson, 2012;). For such purposes, several algorithms have been proposed. What all they have in common, is that they all face challenges representing the natural flow in either concave, convex or plane surfaces (Quin et al., 1991; Burges & Costa-Cabral, 1994; Qin et al., 2007; Pilesjö, 2008).

1.1 Aim and objective

With the wide variety of flow routing methods available, choosing a suitable algorithm is not an easy task. There are multiple factors to consider and the results will vary depending on what method is used. In this study, catchments generated from two flow routing algorithms will be compared, the Deterministic eight-node (D8) algorithm (O'Callaghan & Mark, 1984; Jenson and Domingue, 1988) and the Triangular form-based multiple flow direction algorithm (TFM) (Pilesjö & Hasan, 2014). The D8 method is one of the most debated and criticised flow routing algorithms. This is mainly due to its problems routing the flow through convex and flat surfaces and the substantial generalization of the flow. Despite its known disadvantages, the D8 algorithm is also the most commonly implemented flow routing method of today (Zhao et al., 2009) In contrary to the D8 model, the TFM algorithm has been proven to route through convex, concave and flat surfaces with accurate results. In addition, it can also route through combinations of such surfaces without noticeable artefacts (Pilesjö & Hasan, 2014). The wide recognition of the D8 algorithm and the high accuracy of the TFM model are the main motives when choosing flow routing methods for this analysis. Further descriptions of the models are presented in the background chapter of this thesis.

In this study, the runoff to a single culvert will be estimated to investigate the possible flooding risks. By tracking the flow upslope, the size of the contributing drainage area will be used for calculating the potential 50-, 100- and 200-year flow to the culvert. As watersheds can be delineated manually or digitally, part of the aim of this study is to compare a manually delineated watershed to catchments generated by two different flow-routing algorithms, the deterministic eight (D8) and the Triangle form-based multiple Flow Method (TFM). As DEMs with courser resolution is still widely used today, watersheds will be generated by using six DEMs with varying vertical resolutions. This is done through modifying the vertical resolution by dividing the elevation of the DEM into different vertical intervals to create courser resolution. For further investigation of the watersheds generated by the two flow routing models, three additional culverts are also included in the study.

2. Background

2. 1 Watersheds

In a hilly landscape, topographic ridgelines serve as natural drainage boundaries. A geographical area separated by surrounding ridges is a hydrological unit defined as a watershed. Within the basin all land area contributes its runoff to a common point (Kumar et al., 2015). As water tends to move downwards by the forces of gravity, the common point is normally situated in a watercourse at the bottom of the basin (Wilson, 2012). Because of the physical attributes of the environment, such as topographic and climatic conditions, the characteristics of a watershed will vary (Kumar et al., 2015).

2.1.1 Watershed mapping

The boundaries of a watershed can be outlined manually, for instance by following ridgelines in an aerial photography or a topographic map (Environmental Protection Agency, 1993). In the later example, the ridges are outlined by following contour lines visualizing the ground elevation. The interval between the lines represents the vertical distance. The steepness of the landscape is represented by the horizontal distance of the lines. If the topography is rather flat, the distance between the contours are large, while a steep cliff would result in contour lines with short horizontal distance. When delineating the watershed, the outlines of the watershed should always intersect the contour lines perpendicular (United States Department of Agriculture, 2017).

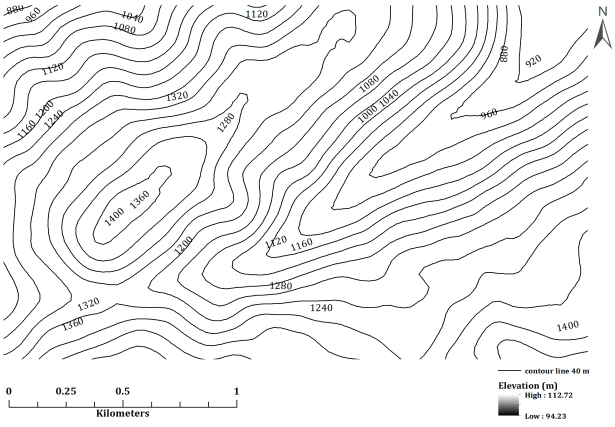

Figure 1. An example of 40 m contour lines representing the elevation of a hilly landscape.

However, modern GIS software often provide watershed extraction tools (Kumar et al., 2015). The accuracy of the modelled drainage divide will partly depend on the resolution of the input (Moore et al., 1991; Meidment, 2002). A watershed can further be divided into sub-catchments based on the hierarchy of the stream channels. As the drainage network within a catchment varies (depending on surface material, local slopes, drainage density etc.), the number and appearance of the sub-catchments will differ. Sub-catchments may also be user induced, by choosing an arbitrary point to make an estimation of estimation the drainage area and flow pattern to that point. A sub-catchment can in its turn be separated into micro-catchments and so forth (Kumar et al., 2015). Sweden is separated into 119 main catchments, which are further divided into more than 50 000 sub-catchments (SMHI, 2012).

2.1.2 Runoff

Runoff can be described as the total volume of surface- and groundwater accumulated from the area to a point at a certain time (SMHI, 2002). The extent of the watershed will partly determine the volume of the runoff. The runoff will accumulate moving downhill, since the contributing land area will increase (SMHI, 2015a). When determining the runoff, the local catchment to a certain point is of interest. Figure 2 illustrates the extent of the contributing land areas starting at a given point (B), located at a higher elevation within the drainage network. By moving the point further downstream (A), the catchment area will increase and enclose all sub-catchments located upstream.

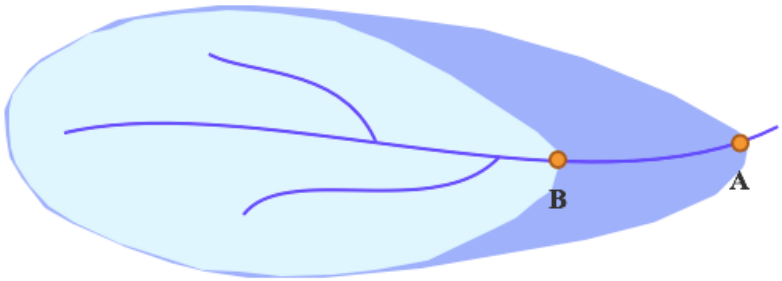

Figure 2. The catchment area of point A will enclose the watershed area of point B. The volume of the runoff at point A will be greater, since point B is located further upstream within the drainage area.

In relation to the local climate conditions, the runoff is depending on several factors, such as evaporation, precipitation and snow melting. The specific catchment runoff is the volume of water transported per surface unit during a given unit of time. In Sweden, the specific runoff differs prominently throughout the seasons and locations. The overall county mean, estimated between year 1961 and 2005, was 12 l/s·km^2. However, comparing the runoff from different locations, it would vary between 4 l/s km^2 and 40 l/s·km^2. The average runoff for Sweden is increasing (SMHI, 2007), although comparing the observations at local levels, the runoff is decreasing in some parts. This is due to warmer winter periods, resulting in less snow cover, leading to lower levels of spring flooding. However, increasing levels of runoff is highly pronounced in the southwest of Svealand, western parts of Götaland and north-western parts of Norrland (SOU, 2007).

2.2 Water discharge along roads

Infrastructure can serve a major impact of the natural drainage systems, by facilitating or cutting the paths of the natural runoff (SMHI, 2015b). The surfaces, which often consist of flat impermeable material, increase peak flows and runoff volumes (Olsson et al., 2016). Therefore, roads and railroads demand a water discharger. To adjust for high runoff flows, artificial drainage systems like culverts and embankments are commonly used along roads and railroads (SMHI, 2015b).

2.2.1 Return periods

When constructing bridges, culverts and embankments possible discharges due to high flows are considered. This is often expressed in their capacity of leading off water charges according to recurrence intervals (Vägverket, 2008). The return period is a statistical estimation of the probability of an event to occur within a given time. Estimations are made from observed data, assuming that the occurrence of an event will not vary over time (SMHI, 2015c). The calculations are based on the highest observed flow within a year. A 50-year flow has a return period of 50 years. This means that the possibility of reaching or exceeding the maximum flow of the observed values is 2 % per year. While the likelihood accumulates with time, the risk of an event to happen is more likely to occur within 50 years than not (table 1).

Table 1. The probability of an event to happen within a recurrence interval accumulates with time (SMHI, 2015c).

Return period	Likelihood to occur within 10 years (%)	Likelihood to occur within 50 years (%)	Likelihood to occur within 100 years (%)
10 years	65	99	100
50 years	18	64	87
100 years	10	39	63

2.2.2 Culverts

A culvert is a pathway located beneath road constructions and serves as an alternative to smaller bridges. They generally have two purposes, serving as an under-road passage for animals and preventing surface water runoff on top of the road (Trafikverket, 2014). The placement of the culvert should be in the direction of the flow, and its angle may not exceed 4% as the runoff volume will increase with steepness. According to Vägverket (2008) the diameter should be at least 0.3 metre, but may not exceed 2 metre. If a culvert bigger than 2 metre is needed, a bridge must instead be constructed. The dimension of the culverts depends on the characteristics of the road and its surrounding local environment. The placement within the landscape, the geometric shape and the traffic load on road is considered. In terrain consisting of uncultivated land, where runoff due to snow melting is highly pronounced, culverts are often sized according to 50-year flows or higher. In urban areas, culverts are sized according to 10-year flows or higher (Vägverket, 2008).

2. 3 Elevation flow routing

The key factors for extracting hydrological information based only on elevation are slope and aspect which can be derived from calculations using local neighbourhood operations. This is generally done by calculating the relation between a centred cell (focus cell) and its adjacent cells, moving a 3x3 gridded window across the DEM (Jenson & Domingue 1988; Qin et al., 2006; Wilson, 2012). Slope and aspect are essential when simulating flow processes. For instance, these factors are used when determining the flow direction and accumulated flow in the catchment. There are two general approaches when calculating the flow direction in a DEM, using either a single flow direction (SFD) or a multiple flow direction (MFD) (Wilson, 2012). These methods will be further described in the upcoming parts of the chapter.

2.3.1 Sinks and flats cells

Flat areas and sinks occur within most DEMs and can complicate the flow routing process. These features can be due to the natural topography, but are usually a result from errors in the source data or in the subsequent handling of these. Artefacts are generally derived by interpolation errors and coarse resolution, creating an in inadequate surface representations (Lindsey, 2015). Coarse resolution, both horizontally and vertically, generalizes the elevation and often fail to represent the natural break lines (Aguilar et al., 2010). Sinks within the DEM can be defined as a depression surrounded with cells of higher elevation, and can consist of multiple cells or a single cell forming a local depression. A 'flat' cell, on the other hand, has zero sloping gradient to its local neighbours. When calculating flow routing paths, sinks can disconnect the drainage (Jenson & Domingue, 1988). Therefore, a DEM is most often prepared by sink filling operations before flow routing in order to ensure the flow. Eliminating artefacts by filling depressions will simultaneously impact the topographic characteristics of the DEM, and filling the sink creates flat areas in which flow directions are problematic to determine (Lindsey & Duhn, 2015). A sink operator can supply the user with an option to fill sinks based on a certain criterion. In ArcGIS the user can specify the maximum depth of a sink that should be filled (ESRI, 2011). In other sink filling operators, such as the TFM model, the user can specify the depth, width or the volume of a sink that is supposed to be filled in the DEM (Hasan et al., 2012). An example of a filling of a sink is presented in figure 3.

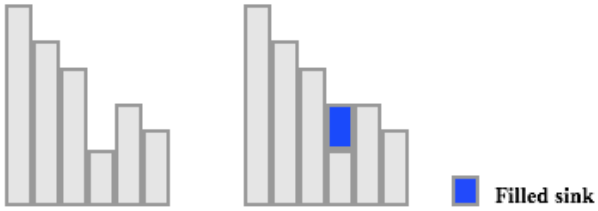

Figure 3. Profile view presenting a filling of a sink within a DEM.

2.3.2 Flow direction methods

Without considering parameters such as surface infiltration or friction, flow directions operations are based only on the elevation stored in the raster cells. The direction of the flow is depending on the local maximum downslope gradient (Moore et al., 2001, Wilson, 2008). There are multiple ways to address the issue; some flow direction algorithms treat cells as point sources, assuming that the water flows from the centre of each cell (O'Callaghan & Mark, 1984; Jenson & Domingue, 1988). Alternative methods rather treat the cell as a continuous area, dividing it into gridded or triangular irregular networks (TIN) surfaces. This allows the flow to split into multiple directions. The results of the outputs, such as flow accumulation, upslope contributing area etc., will differ depending on which flow routing method is used (Moore et al., 1991; Burges & Costa-Cabral, 1994; Garbrecht & Martz, 1996; Wilson et al., 2008; Pilesjö & Hasan, 2014).

2.3.2.1 Single flow direction and multiple flow direction

The main difference between the SFD and the MFD methods is in the number of adjacent cells that can receive output flow from the focusing cell (Wilson, 2012) as presented in figure 4. SFD algorithms allow the flow to move in one of eight possible directions, towards the neighbouring cell with the steepest decent. Since SFD algorithms are unable of modelling divergent flow, this becomes a problem when routing through convex and plane surfaces. Many MFD methods have been established in attempt to overcome such limitations, by allowing the flow from the focus cell to split into two or more adjacent cells. However, many MFD algorithms have problems representing the flow on concave surfaces when the water is converging (Quinn et al., 1991; Costa-Cabral & Burges 1994; Tarboton, 1997; Zhao et al., 2009; Pilesjö & Hasan, 2014).

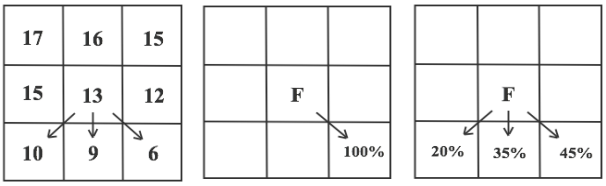

Figure 4. Based on the elevation in the cells of the input raster (left), the direction of the flow can be routed into single (middle) or multiple (right) cells depending on the algorithm.

2.4 Deterministic eight-node algorithm (D8)

One of the commonly used raster-based SDF algorithms today is the deterministic eight-node algorithm (D8), first introduced by O'Callaghan & Mark (1984), and was further improved by Jenson and Domingue (1988). Due to its simplicity and its efficiency deriving hydrological features, the D8 algorithm is used in today's ArcGIS software (ESRI, 2012a). In the D8 model, cells are treated as points located in the centre of each cell. Slope gradients in each direction will be determined by calculating the point-to-point relationship from the centre of the focusing cell to the centre of its adjacent cells. As the possible flow directions will be either cardinal or diagonal, the potential routes are 0°, 45°, 90°, 135°, 180°, 225°, 270°, 315°, counted clockwise from the north (Jenson & Domingue, 1988). The flow direction can in a simple sense be described by the equation:

$$Flow\ Direction = \Delta Z\ /d \tag{1}$$

where delta Z is the elevation drop and d is the distance.

Explained further, the direction of the flow is determined through weighting of the slopes. The weighted values are derived by calculating the elevation difference divided by the distance between each cell and its eight neighbours. Cells located in the edges of the raster only will automatically be given a flow direction out of the DEM. The direction of the flow is decided based on the slope with the maximum slope gradient. If the slope gradient is zero in all directions, the cell is a member of a flat area. In this case, the elevation of the neighbouring

cells is subtracted from the focus cell and divided by the distance to the centre of the neighbours. If the difference in elevation is negative, it will not be given an outflow direction as it is a sink (Jenson & Domingue, 1988).

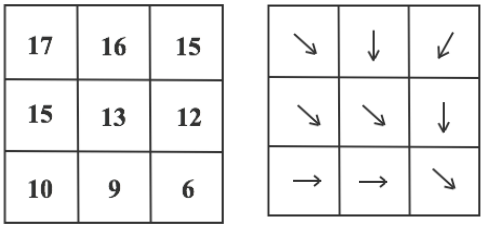

Figure 5. The direction of the flow (right) will be directed into the neighbouring cell with the lowest elevation (left)

After the direction is defined, the focus cell will be encoded, giving it a value corresponding to the location of recieving cell (figure 6).

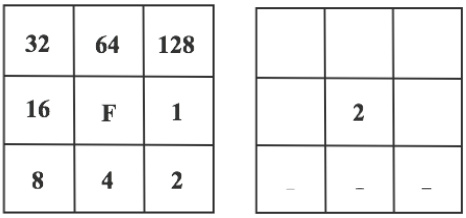

Figure 6. The encoding of the focus cell (left) is calculated by the corresponding location of the inflow cell (right).

2.5 Triangular Formed-based Multiple flow algorithm (TFM)

Several MFD methods have been designed in purpose to overcome the limitations of the SFD algorithms. One of such methods is the Triangular formed-based Multiple Flow algorithm (TFM), initiated by Pilesjö and Hasan (2014). To divert the flow into multiple directions, the TFM model applies TIN surfaces with constant slope and aspect. The model implements a stepwise procedure. Firstly, all cells in the raster is divided into eight equally sized triangles (facets). The facets are calculated using Pythagoras theorem, using the centre of the focus cell (M) and the centre of its neighbours (C1 and C2), presented in figure 7. As each facet is defined, constant slope and aspect are also determined (Pilesjö & Hasan, 2014).

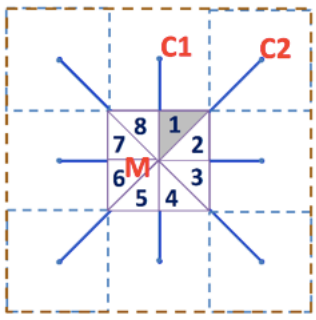

Figure 7. In the first step, the focus cell is divided into eight equally sized facets (1-8). By using the centre points of the neighbour cells (C1 and C2) and the centre of the focus cell (M), the facets can be calculated through Pythagoras theorem (Pilesjö & Hasan, 2014).

In the next step, planes are calculated for each facet, as the slope and aspect are continuous. The surfaces are derived by using the vertex coordinates of the facets (Pilesjö & Hasan, 2014). If the focus cell has no slope gradient to its adjacent cells, the TFM algorithm will identify the outlet as the cell with lowest elevation outside the boarder of the flat area. A vector file is added to the cells, with the corresponding direction of the outlet, assigning the cells an artificial slope. This allows the flow to divert within plane areas (Hasan et al., 2012).

The third step involves routing of the flow within the cell, imagining there is a portion of water that is distributed between the facets. The water can move in three possible ways between the facets, denoted as *split*, *move* or *stay*, which is depending on the aspect. If the flow can go directly into a neighbouring cell, i.e. without routing to any other facet, it fulfils the condition of *stay*. If all the water within a facet can be routed to only one other facet, it will be denoted as *move*. However, if the flow between two facets is directed towards each other, in convergent directions, they will be denoted as *stay*. Otherwise the condition, *split*, is denoted (Pilesjö & Hasan, 2014). The possible movements are further illustrated in figure 8.

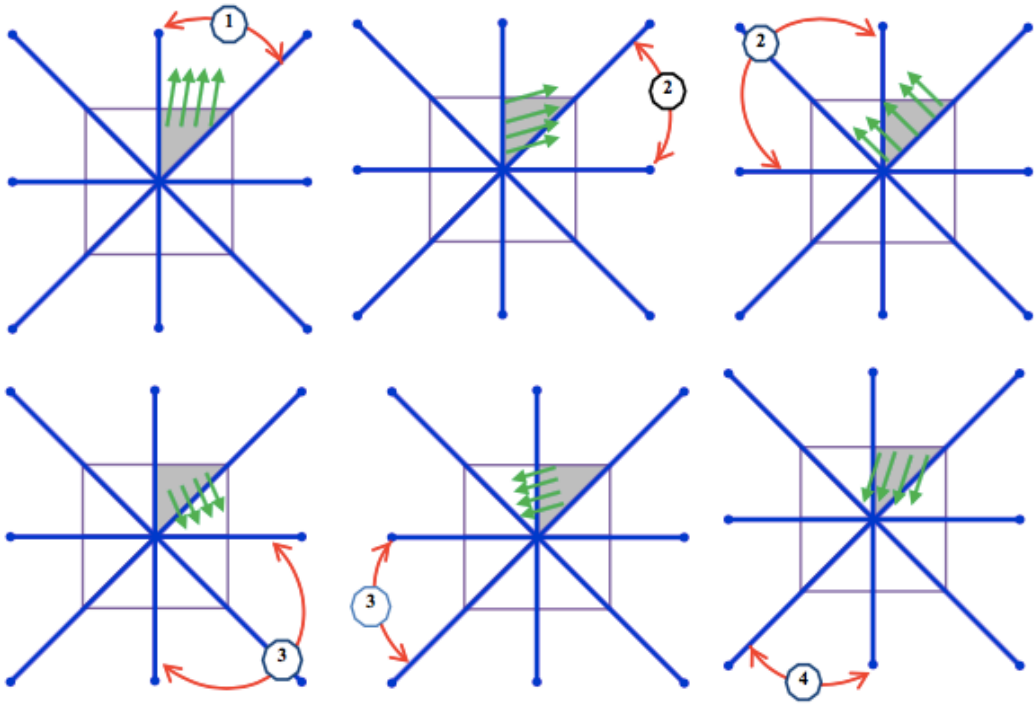

Figure 8. The possible directions for the water to move between the facets within the focus cell. The portion of water in the facet (grey) can either stay (1), split (2 and 4) or move (3) depending on the aspect (Pilesjö & Hasan, 2014).

The distribution of water portions between the facets will vary depending on the shape of the terrain. If the cell has a convex slope, the water will be distributed into all facets. A cell has a concave slope, all portions of water into a single facet. For an instance, if the cell is a sink it has a concave slope and all water would be sorted into a single facet. The final step consists of routing the flow towards one or more adjacent cells. The direction of the flow will be distributed according to the portions of accumulated water amongst the facets. Each facet has two neighbouring cells, and if the facet contains any water this will be distributed to 1, 2 or 0 neighbours based on the slope. For instance, the flow distribution from facet 1 (figure 7) to its neighbours C1 and C2, will be divided according to box 1 below.

1 - C1 has lower elevation than C2, but the elevation of C2 is equal or higher than facet 1 - All water within the facet will be distributed to C1.

2 - C1 and C2 have lower elevation than facet 1 - The accumulated water within the facet will be proportionally distributed between C1 and C2.

0 - Both C1 and C2 have equal or higher elevation than facet 1, and the remaining adjecent cells have lower elevation - The accumulated water within the facet will be proportionally distributed to the rest of the facets within the focus cell.

Box 1. The alternatives of flow distribution from facets 1 to its neighbours C1 and C2.

2.6 Flow accumulation

Datasets of flow direction can be used as a tool identifying drainage networks by calculating the accumulated flow. This is done by counting the number of cells contributing to the downstream flow. Each cell within the raster will be given a value depending on the number of cells that flows in its direction (ESRI, 2016). If a cell has no contributing flow from its neighbours, it will be given a certain value (0 for the 'flow accumulation' operator ArcGIS and 1 for the TFM model). An output dataset for the D8 method is presented in figure 9.

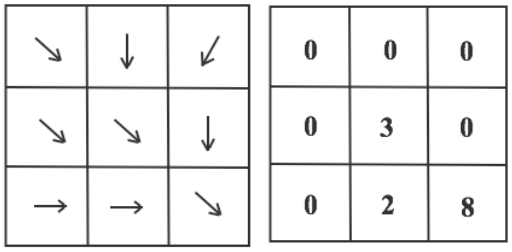

Figur 9. Depending on the flow direction of the cells (left), the accumulated flow (right) is done by counting the cells contributing to the downstream flow.

2.7 Up-tracking – Watershed boundaries

The flow direction raster is not only used for calculating the accumulated flow, but also for deriving watershed boundaries (Wilson, 2012). Rather than tracking the flow downhill, watersheds are derived by tracking the flow in an upslope direction. This generally demands for the user to supply a point, a 'receiving cell', or the row and column number for the specific cell.

The D8 algorithm generates a single flow direction dataset which consist of encoded values. Only neighbouring cells encoding in the direction of the focus cell will be accounted for (ESRI, 2017). The TFM flow direction dataset consists of values describing the amount of water flowing from a cell in percentage. If the neighbouring cell has a value bigger than 0, it is a part of the watershed. For both methods, the up-tracking function will divide the cells into two classes. TFM method, the value of 1 will be given to contributing cells and 0 for non-contributing cells (figure 10). From the start, all cells in the output raster will be given the number of 0, except for the receiving cell, which will be given the number of 1. The up-tracking starts from chosen cell, examining the flow direction of its eight surrounding neighbours. If an adjacent cell has a flow direction towards the current cell, it will be assigned as 1 in the output dataset. Otherwise, the corresponding cell in the output raster will remain as 0. This process will continue recursively for all cells defined as members of class 1, until inflowing cells are exhausted for the receiving cell.

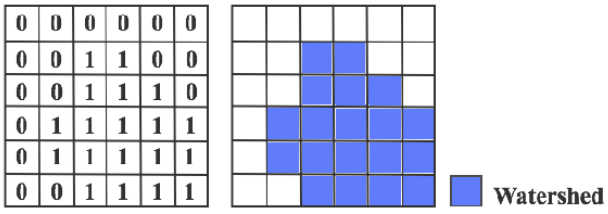

Figure 10. Cells contributing to the catchment area will be assigned the number of 1, while non-contributing will be assigned the value of 0.

3. Methodology

3. 1 Data and software

To conduct this study the ArcGIS 10.3.1, MATLAB 2015b and Microsoft Excel software was utilized. GSD-Elevation data *Grid2+* was retrieved from the Swedish land surveys' geodata service in ASCII-format. The spatial resolution of *Grid2+* is 2 meters horizontally and 0,05 meters in vertical direction (Lantmäteriet, 2016b). A polyline layer of sections, indicating culvert positions, was provided by the Transport Administration, as well as polygon layers of the catchments covering the study area of Vederslöv. To further locate the position of the culverts, an orthophoto with a resolution of 0.5 metre was retrieved from the Swedish land survey.

Data covering the Swedish county boundaries was retrieved from ArcGIS (2012) in shapefile format. Shapefiles covering the main- and sub- catchments of Sweden was retrieved from Swedish Metrological and Hydrological Institute, along with future scenario data of the mean annual average runoff. The runoff data consisted of three datasets, observed mean annual runoff from 1962 to 1992, and two future scenarios RCP4.5 and RCP8.5. The representative Consecration Pathways (RCP) scenarios demonstrate the possible future radiation evolvements. In the RCP4.5 dataset, greenhouse gas emissions will peak at year 2040, estimating a radiative forcing value of 4.5 W/m^2 in the year 2100. In the RCP8.5 scenario, emissions will increase throughout the century, predicting a radiative forcing value of 8.5 W/m^2 (SMHI, 2015d). All data had the spatial reference system SWEREF99 TM.

3. 2 Study site

Vederslöv is one of the 13 districts in Växjö municipality, located in Kronobergs county (figure 11). The sparsely populated parish mainly consists mixed forest, cultivated land and pastures. Throughout the area, a network of streams is converging into a lake, Vederslövssjön, situated in the southern part of the district (Länsstyrelsen, 2017). Vederslövssjön is a part of the sub-catchment area 'The outlet by Vederslövssjön', which in its turn is a part of Mörrumåns main catchment area (SMHI, 2012).

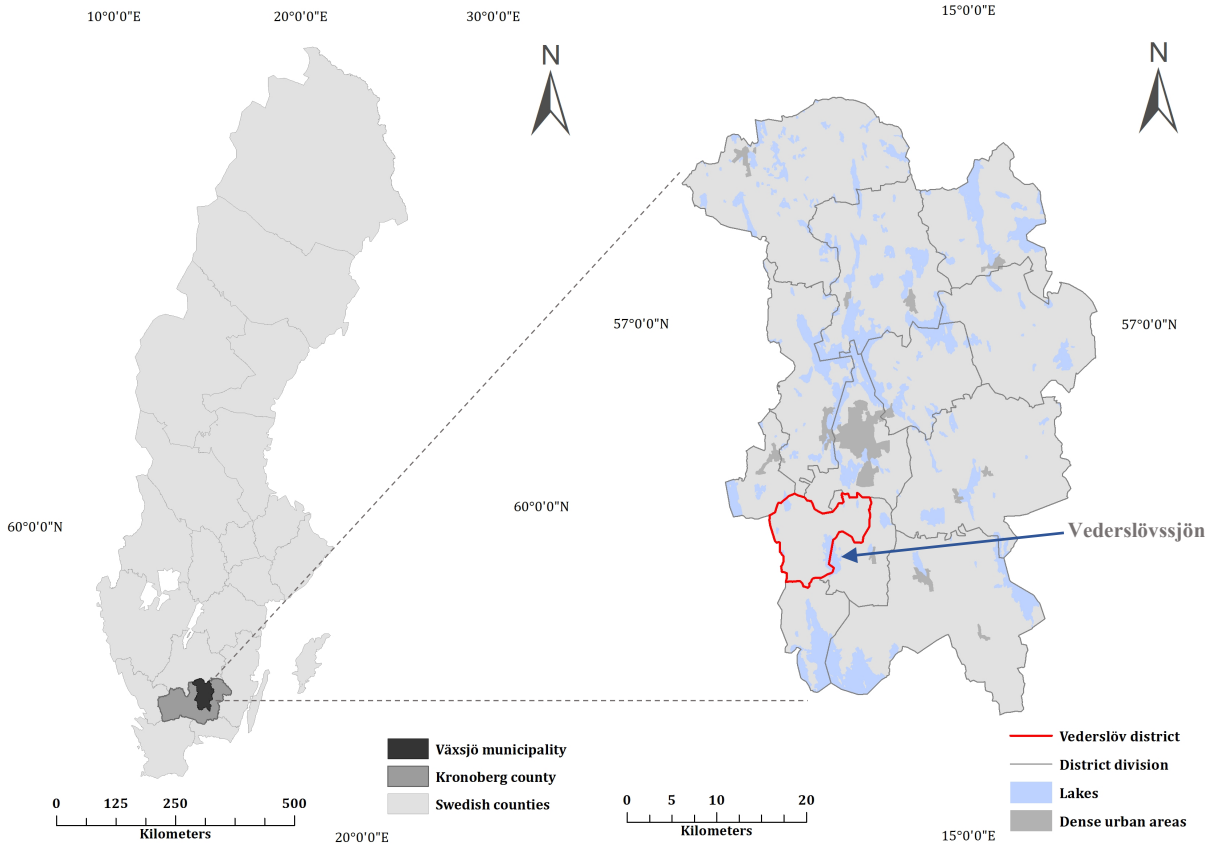

Figure 11. Växsjö municipality if located in Kronobergs county, in the south-centre part of Sweden. Outlined in red is the district Vederslöv, which is one of Växsjö's 13 districts. Vederslövssjön is located in the south part of Vederslöv.

Road 696 stretches throughout the district and passes by the top of Vederslövssjön. As the road crosses the flow towards the lake, a culvert is placed across this section (figure 12). Information about the culvet was retrieved from the city planning office in Växsjö municipality. The culvert has an inner diameter of 900 mm and a total length of 7.75 m. The elevation at the inflow is 159.75 m and the outflow is 159.26 m. To estimate a 50year runoff to the culvert, the watershed to the culvert was manually delineated by consultants at Metria on behalf of the Traffic Administration, figure S1 (see appendix 1). The delineation of the ridgelines along the catchment was defined utilizing a topographic map with 5-metre contour lines. The catchment was further measured by using a planimeter.

For further comparison of watersheds generated by the models, catchments for three neighbouring culverts was also included as a sub-study. Two of the culverts are located along road 697, which stretches along the watershed belonging to main culvert, and intersect with road 696 on top of the lake. The third culvert is located on road 696, approximately 200 m west from the main culvert.

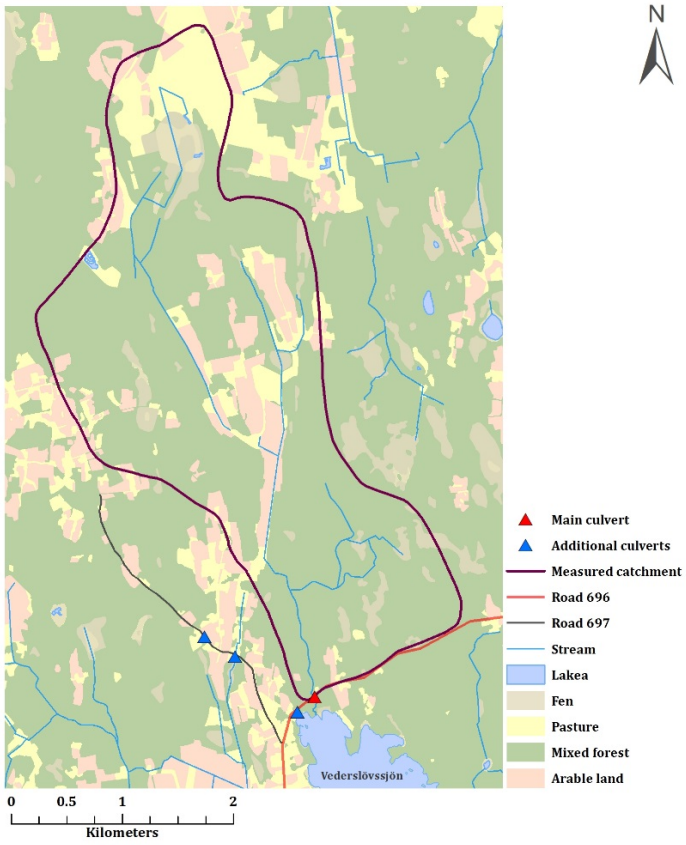

Figure 12. The manually measured catchment area (brown) to the main culvert (red), crossing road 696, connecting the stream channel to Vederslövssjön. The additional culverts, along road 697 and 696, are presented in blue.

According to the two future scenarios RCP4.5 and RCP 8.5, expected changes in climate for Kronobergs county will contribute to an increase in the annual average temperatures. Alterations in the annual precipitation pattern are also indicated, causing an increase in the levels of rainfall throughout the year. The predicted annual average runoff, which also will increase (table 2), will be highly pronounced during the winter (SMHI, 2015c).

Table 2. Changes in the average annual runoff for the sub-catchment 'Outlet by Vederslövssjön'. The values are estimated by comparing the two climate scenarios RCP4.5 and RCP8.5 to the reference period 1962-1992. (SMHI, 2015d).

Scenario	2021 – 2050 (%)	2069 – 2098 (%)
RCP 4.5	3,0	5,1
RCP 8.5	3,8	6,6

3. 3 Modifying the vertical resolution

The vertical resolution of the DEM was modified using MATLAB2015b software. A DEM with 0,05m vertical resolution, was used as input, from which the total number of rows and columns was derived and stored in separate vector files. An output matrix, filled with zeroes, was created based on the rows and columns sizes. The minimum and maximum cell value was derived from the input DEM and stored in separate vectors. To create vertical breaks, elevation classes were determined for each interval. The division of the classes was done by starting at the minimum elevation value and spaced by the given interval, until it reached the maximum elevation. By looping through the elevation matrix, each cell could be compared with the classification vector. The cell value would fit into a certain elevation class, which the

corresponding cell in the output matrix would receive. The process is presented in the flow chart below. In total, 5 DEMs were created with 0,01m, 0,10m, 0,25m, 0,50m and 1m intervals.

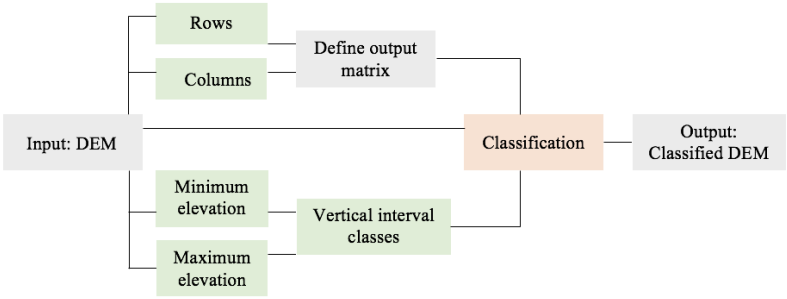

Flow chart 1. A DEM with 0,05 m vertical resolution was used as input. The grey colours represent matrixes, while green colours are vectors. The orange box represents the classifications done by looping over the DEM, using the classification vector and the empty matrix to create an output DEM.

3. 4 Deriving watersheds

The delineated catchment area in Vederslöv was retrieved in a PNG-format and needed to be digitalized. The background map of the area, onto which the catchment had been sketched, was a terrain map with houses, roads, contour lines ect. Together with the features in the terrain map and an ortophoto, figure S2 (see appendix 2), the catchment could be digitalized in ArcMap. The positions of the culverts were located using the ortophoto, as their inflow was connected to the stream channels. The watersheds for the D8 model was derived using the hydrology tools available in ArcMap, shown in the flow chart below.

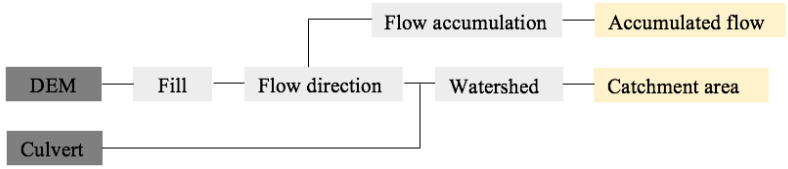

Flow chart 2. The workflow of generating a catchment areas for the D8-model. Dark grey represents input files, while lighter grey are the hydrology tools utilized. The output is presented in orange.

The TFM model was scripted in MATLAB and consisted of multiple m-files. The main script used the original DEM as input and called for the external functions to fill sinks, calculate slope and aspect, accumulate the flow, and to calculate the catchment area (flow chart 3).

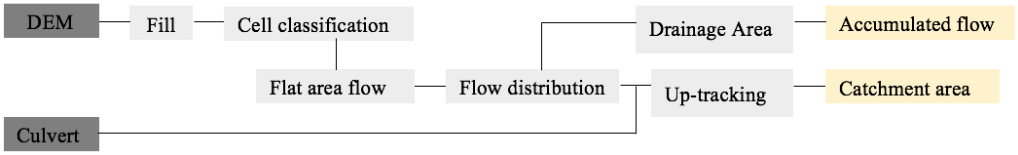

Flow chart 3. The workflow of the TFM model. The user supplies the input (dark grey), and the main script call for the external functions (light grey). The output layers are presented in orange.

The watersheds derived by the TFM model was further examined in ArcMap and compared with the results from the D8 algorithm. In addition to the visual comparisons, the difference in number of cells were extracted by subtracting the layers using the 'raster calculator' operator in ArcMap. The difference in area was obtained by multiplying the cells with 4, since the cell size of the raster was 2x2 meter. The sizes of catchment were further analysed by statistical t-tests to detect any significant differences within the results.

3.5 Runoff estimation

The runoff of a catchment area is influenced by the specific runoff, catchment size and lakes within the area. Estimations of a 50-, 100- and 200-year flow to the culvert in Vederslöv were based on equations given by Vägverket (2008). The HQ is an estimate of the highest flow (m^3/s) for a return period. The mean annual catchment runoff (*MQ*) observed under the recurrence period is estimated in m^3/s by equation 4,

$$MQ = (Mq \cdot N \cdot 10^{-3}) \cdot (1 - P) \quad (4)$$

where *Mq* is the estimated specific runoff (l/s km^2), *N* is the size (km^2) of the catchment and *P* is the percentage of lakes within the sub-catchment area. The estimated *Mq* value for the area is 9 l/s km^2 (Vägverket, 2008). *MQ* was further used to calculate the mean runoff of the year with highest observed runoff (m^3/s) within the period (MHQ):

$$MHQ = i + MQ \quad (5)$$

where *i* is a correction adjusting for possible future changes in the mean annual runoff of the catchment (*MQ)*. The adjusting value was 1.1 for catchments located in the Vederslöv area (Vägverket, 2008). The highest flow within the recurrence interval (HQ) was estimated for 50-years according to equation 6,

$$HQ_n = k \cdot MHQ \quad (6)$$

where *n* is the number of years and *k* is the recurrence factor, which depends on the presence of lakes. The *k* factor had a value of 3 for a 50-year flow. Estimations of HHQ_{100} and HHQ_{200} was done by multiplying HHQ_{50} with 1,1 and 1,2.

3.6 Maximum flow capacity of the culvert

As the diameter, length and the elevation of the in- and outlet of culvert was known, the flow capacity of the culvert when filled could be calculated through equation 7 (Statens planverks författningsansamling, 1980). The maximum flow rate (Q_{max} m^3/s) can be described as:

$$Qmax = 6.75log\left[\left[\frac{0.74}{d\left(\sqrt{d \cdot j}\right)\cdot 10^6} + \frac{n}{3.71 \cdot d}\right]\right] d^2 \cdot \sqrt{d \cdot j} \quad (7)$$

where *d* is the inner diameter of the culvert (m), *n* is the roughness coefficient of the material (m) and *J* is the slope (m/m). The roughness coefficient (*n*) for concrete was 0,001 m according to Statens planverks författningsansamling (1980).

4. Results

The resolution was modified for five DEMs. The DEM used as input had a vertical resolution of 0,05m, which from now on will be referred to as the 'original DEM'. The comparison of the manually delineated watershed to the original DEM is presented in figure S3 (appendix 3). The layers produced in vertical modification is presented in figure S4 – S9 (appendix 4), along with layers of accumulated flow presented in figure S10 – S21 (appendix 5).

4.1 Watersheds

In total, 6 catchments to the main culvert by Vederslövssjön were derived respectively from the TFM and the D8 model using original DEMs, and DEMs with vertical intervals of 0,01m, 0,10m, 0,25m 0,50m and 1m. The modelled watersheds were further compared to one another, and to the manually measured catchment, separately.

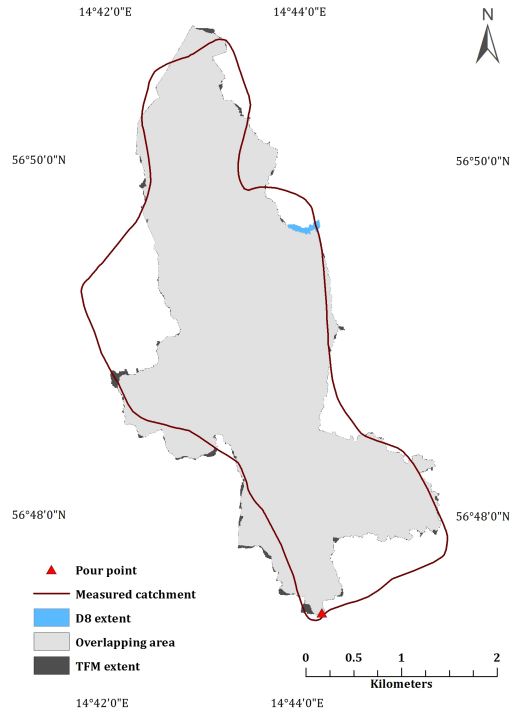

Figure 13. Differences between the watersheds derived by using the original DEM. The manually measured catchment is outlined in brown. The parts of the catchments extending from the overlapping area (light grey) are presented in blue (D8) and dark grey (TFM).

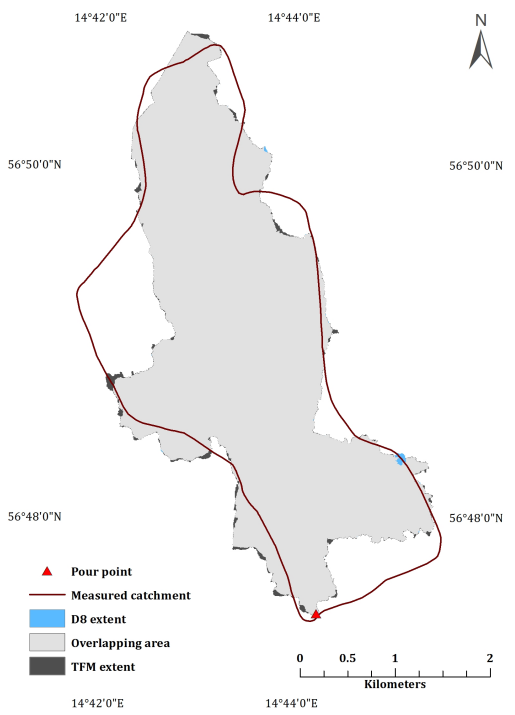

Figure 14. The catchments differences derived by using a DEM with 0,01m vertical interval. The manually delineated watershed is outlined in brown. The cells extending from the overlapping area (light grey) are presented in blue (D8) and dark grey (TFM).

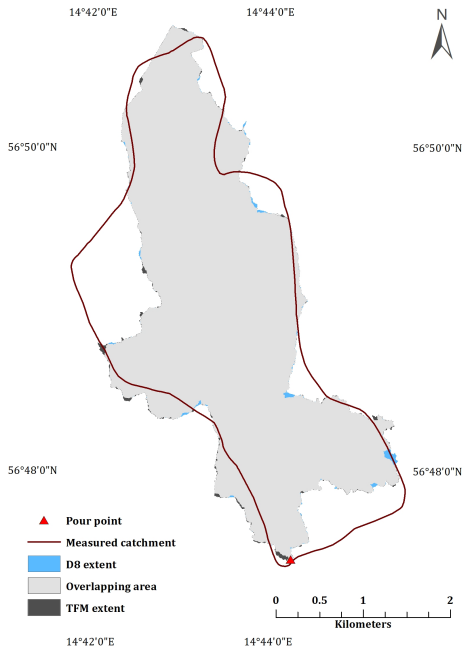

Figure 15. Differences between the watersheds derived by using a DEM with 0,10m vertical interval. The manually measured watershed is outlined in brown. The parts of the catchments extending from the overlapping area (light grey) are presented in blue (D8) and dark grey (TFM).

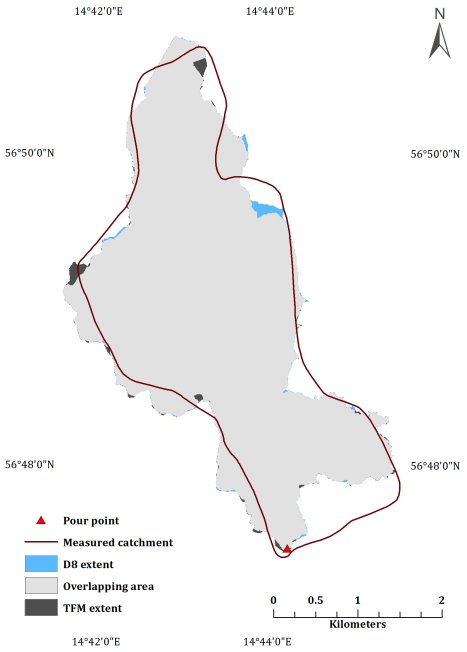

Figure 16. The catchments differences derived by using a DEM with 0,25m vertical interval. The manually delineated watershed is outlined in brown. The cells extending from the overlapping area (light grey) are presented in blue (D8) and dark grey (TFM).

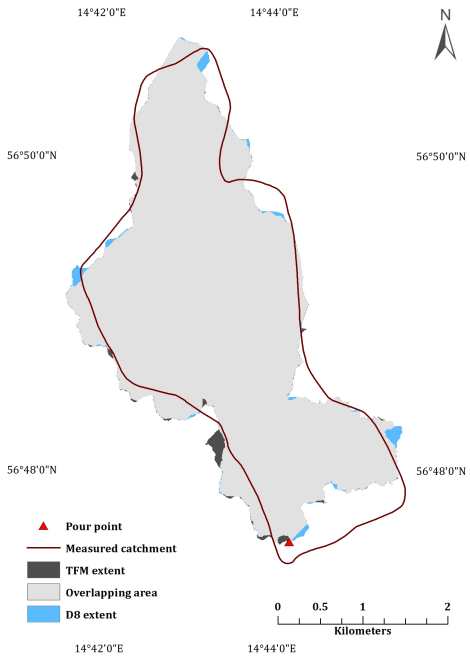

Figure 17. Differences between the watersheds derived by using a DEM with 0,50m vertical interval. The manually measured watershed is outlined in brown. The parts of the catchments extending from the overlapping area (light grey) are presented in blue (D8) and dark grey (TFM).

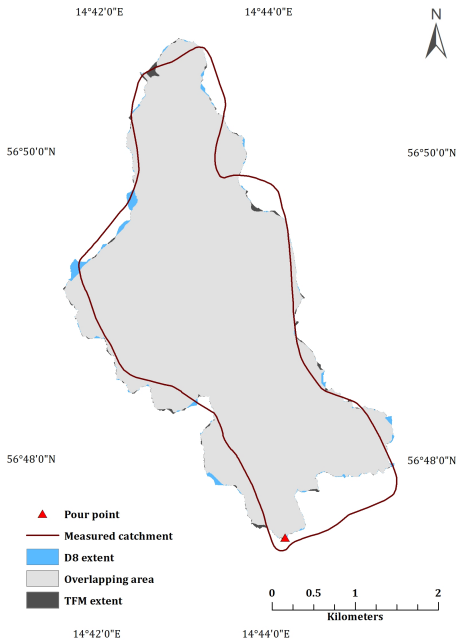

Figure 18. The catchments differences derived by using a DEM with 1m vertical interval. The manually delineated watershed is outlined in brown. The cells extending from the overlapping area (light grey) are presented in blue (D8) and dark grey (TFM).

The characteristics of the catchments from the D8 and the TFM model depend on the DEM used as input. Resemblances in size, shape and location are prominent, comparing the modelled catchments to one another for separate DEMs tested. The manually delineated catchment does not always deviate in size (figure 19) but in shape, without exception, comparing it to the modelled watersheds. This is mainly pronounced for the catchments modelled with DEMs with higher resolution (figure 13, 14, 15). Watersheds derived with large intervals (figure 16, 17, 18) will expand further in north-western direction, forming a greater resemblance to the manually measured catchment.

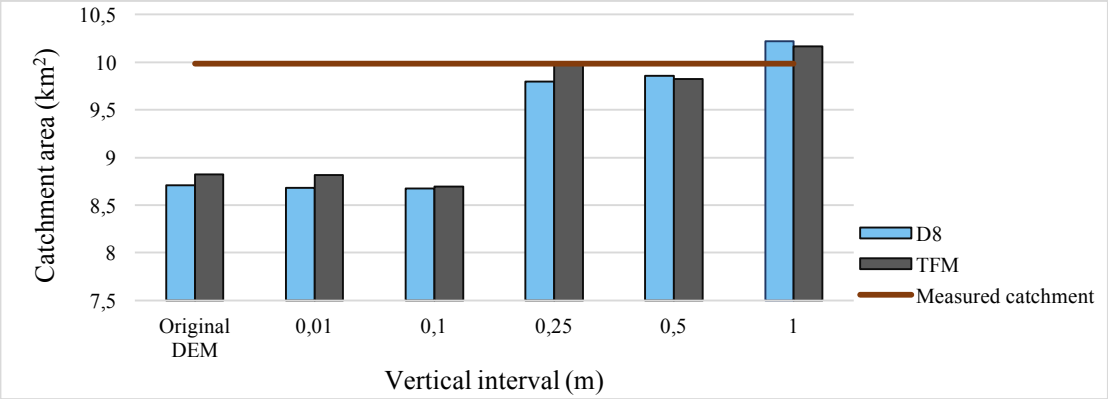

Figure 19. The size of the catchment areas produced by the D8 (blue) and the TFM (grey) algorithms using DEMs with different vertical intervals. The size of the manually measured catchment is presented by the brown line.

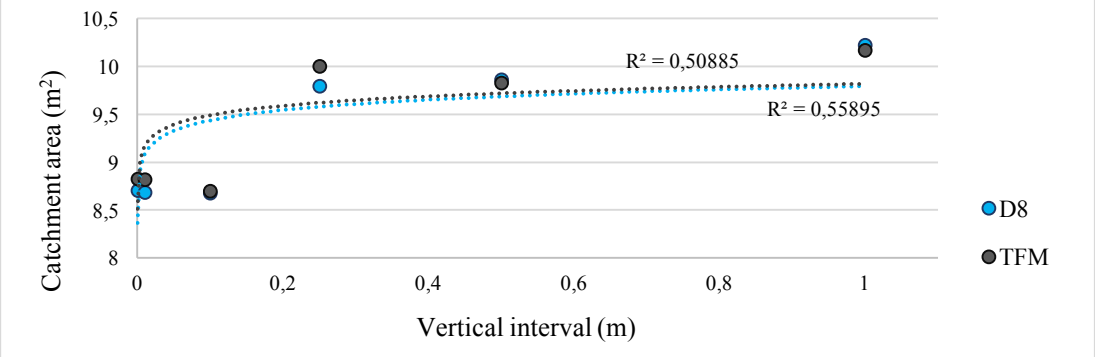

Figure 20. Correlation between the catchment area (y-axis) and the vertical resolutions of the DEMs (x-axis). The positive logarithmic trend lines indicate moderate correlations for both models. The r^2 value received for the D8 watersheds is 0,55895, while the r^2 value for the TFM catchments is 0,50885.

Plotting the number of cells against the vertical resolution, the modelled watersheds will expand with increasing distance along the z-direction (figure 20). The total watershed area yield by the TFM model is 56,3 km^2 and 55,9 km^2 for the D8 model (table 3), when adding the catchments together for each model separately. This means that the D8 model produces 0,8% smaller catchments in total. Due to the minor difference in size and shape, the modelled cells share 98,9% of their overlapping cells in total. Plotting both the number of cells against the number of overlapping cells (figure 21), this is further evident. However, the number of cells exceeding the overlapping area differ between the models when the vertical distance increases (figure 22). For DEMs with higher vertical intervals, the D8 cells stretch further beyond the common area than the TFM cells. Using DEMs with low vertical intervals, the TFM cells stretch further beyond the overlapping area than the D8 cells.

Comparing the size of the modelled catchments to the manually measured, the models produced approximately 6,3 % smaller watersheds in total (table 3). The total number of overlapping cells are 86,0% for the D8 catchments and 86,2% for the TFM catchments, meaning most of the modelled cells are within external border of the manually delineated watershed. The number of overlapping cells increases as the sizes of the modelled catchments are expanding (figure 23 and 24). The number of cells exceeding the overlapping area will decrease for the measured watershed when the vertical interval gets higher (figure 24 and figure 26), suggesting that modelled catchments will extend further beyond the measured border as the resolution gets lower.

Table 3. The total catchment area, for all DEMs tested, compared to combined area of the watersheds. The modelled catchments are both compared to one another, and to the manually measured catchment, separately.

	Area (km^2)	Percentage of combined area (%)
TFM - D8		
TFM	56,3	50,2
D8	55,9	49,8
Overlapping	111,0	98,9
Combined	112,3	
TFM - measured catchment		
TFM	56,3	48,5
Measured catchment	59,9	51,5
Overlapping	100,0	86,0
Combined	116,2	
D8 - measured catchment		
D8	55,9	48,3
Measured catchment	59,9	51,7
Overlapping	99,9	86,2
Combined	115,8	

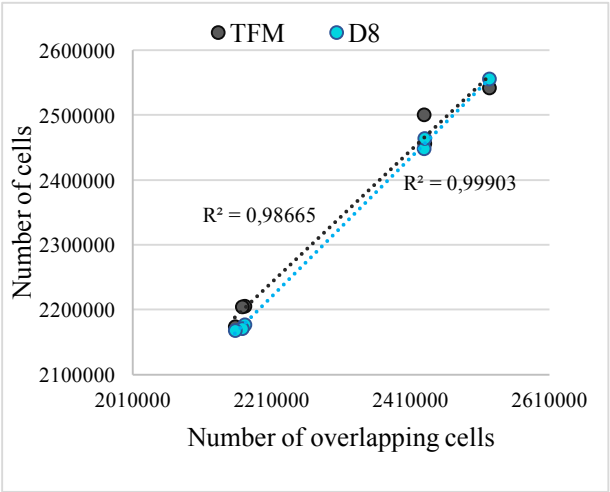

Figure 21. The correlation between the number of cells (y-axis) and the number of overlapping cells (x-axis). The r^2 value indicates strong correlations for both the D8 ($r^2 = 0,99903$), and the TFM model ($r^2 = 0,98665$), based on the linear trend lines.

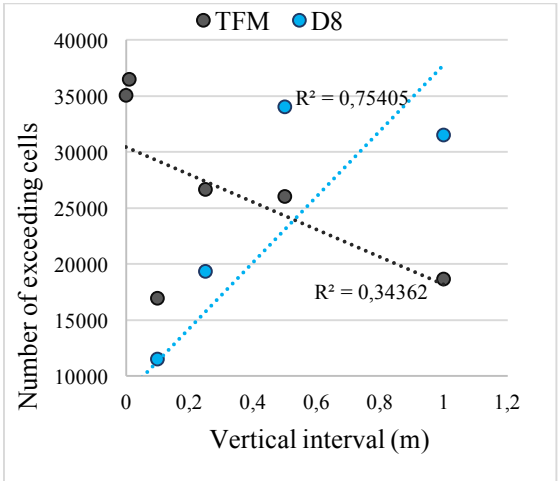

Figure 22. Correlation between the number of cells exceeding the overlapping area (y-axis), plotted against vertical interval (x-axis). The linier trend lines retrieve a moderate r^2 values for the D8 model ($r^2 = 0,75405$) and for the TFM model ($r^2 = 0,34362$).

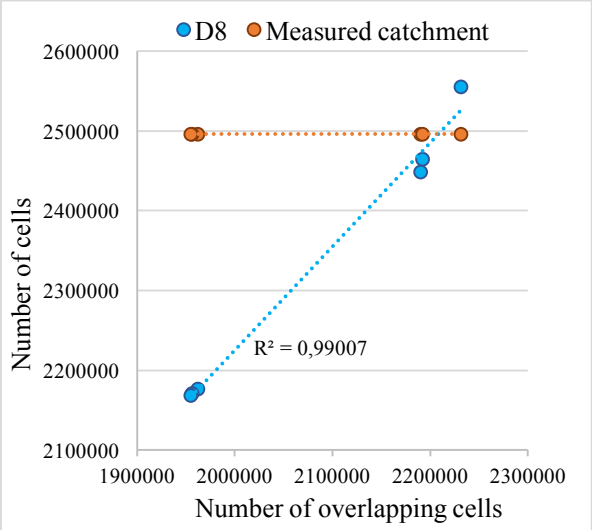

Figure 23. The correlation between the number of cells (y-axis) and the number overlapping cells (x-axis), comparing the D8 catchments to the manually measured catchment. The linear trend line for the D8 model indicates a strong correlation (r^2 = 0,99001).

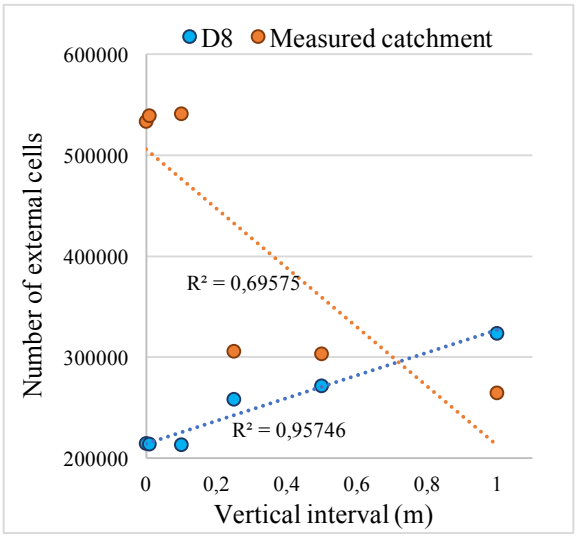

Figure 24. Correlation between the of the number of cells exceeding the overlapping area (y-axis) and the vertical interval (x-axis), comparing the D8 watersheds to the manually measured catchment. A high r^2 value (0,95746) is retrieved for the D8 catchments, while the r2 value for the measured watershed is moderate (r^2 = 0,69575).

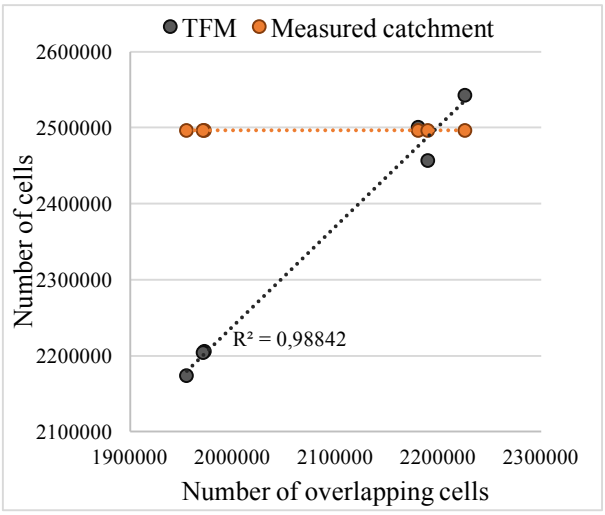

Figure 25. Correlation of the number of cells (y-axis) and the number of overlapping cells (x-axis), plotting the TFM model and against the manually measured catchment. Based on a linear trend line, strong correlation is pronounced for the TFM model (r^2 = 0,98842).

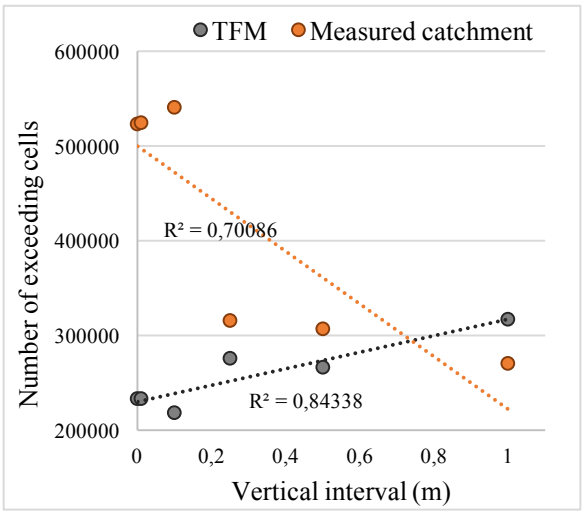

Figure 26. The correlation between the number of cells exceeding the overlapping area (y-axis) and vertical interval (x-axis), plotting the TFM model against the manually measured catchment. The r^2 value for the TFM model is 0,84338, while the r^2 value for the measured watershed is moderate (r^2 = 0,70086).

The area of the watersheds was further analysed by single and paired t-tests to detect any significant differences within the results (table 4). Comparing the catchments generated from the D8 and TFM model to one another, and to the manually measured catchment separately, no significant difference was found ($p < 0,05$).

Table 4. Results from the modelled watersheds are compared with a paired t-test. The size of the manually measured catchments are separately tested for each model with single t-tests.

	α	*n*	*df*	Mean μ	SD σ	t calculated	t critical	*p*
TFM - D8	0,05	6	5	16387,8	19037,7	2,108	2,571	<0,05
D8 - Measured catchment	0,05	6	5	2347013,3	2020018,5	2,543	2,571	<0,05
TFM - Measured catchment	0,05	6	5	2330625,5	1992633,2	2,558	2,571	<0,05

4.2 Watersheds derived to the additional culverts

Catchments to three additional culverts, located along the main catchment, were created using the original DEM with 0,05 m vertical resolution. The watersheds from the additional culverts merged together with the watershed from the main culvert are presented in appendix 6.

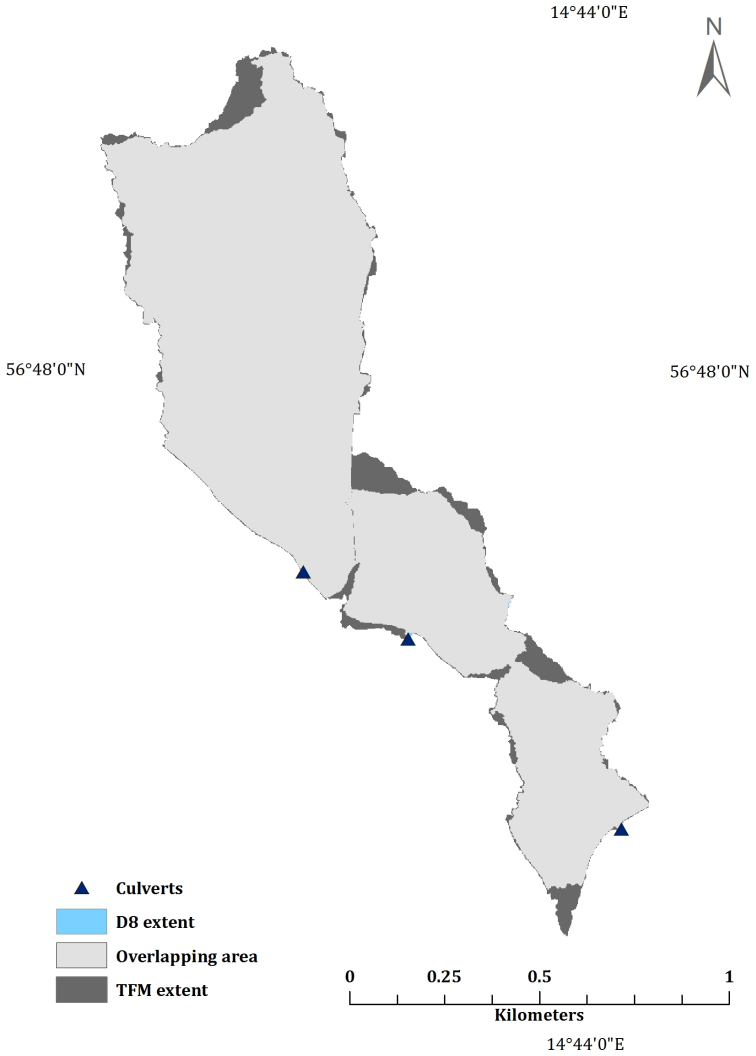

Figure 27. Watersheds to the additional culverts derived by using a DEM with 0,05m vertical resolution. The overlapping cells are presented in light grey, while cells exceeding the common area are presented in dark grey (TFM) and blue (D8)

Merging the catchments together, for each model separately, and visually comparing them differences are noticeable regarding the size and shape. Most of the D8 cells are contributing to the overlapping area. It appears that the D8 cells are enclosed by the TFM cells, extending the catchments further.

4.3 Runoff to the main culvert

The highest peak discharge for the stream flow is depending on the size of the watershed, the specific runoff and the presence of lakes within the area. The 50-, 100- and 200-year flows to the culvert was estimated models according to equation 4, 5 and 6. The runoff is calculated to a single culvert, meaning the specific runoff and the lake percentage is equal for all calculations. The maximum capacity of the culvert was derived according to equation 7, and is based on the information about the length, the diameter, along with the elevation of the in- and outlet. To investigate if the culvert is potentially undersized, the maximum capacity of the culvert is set as a threshold for each of the calculated flows.

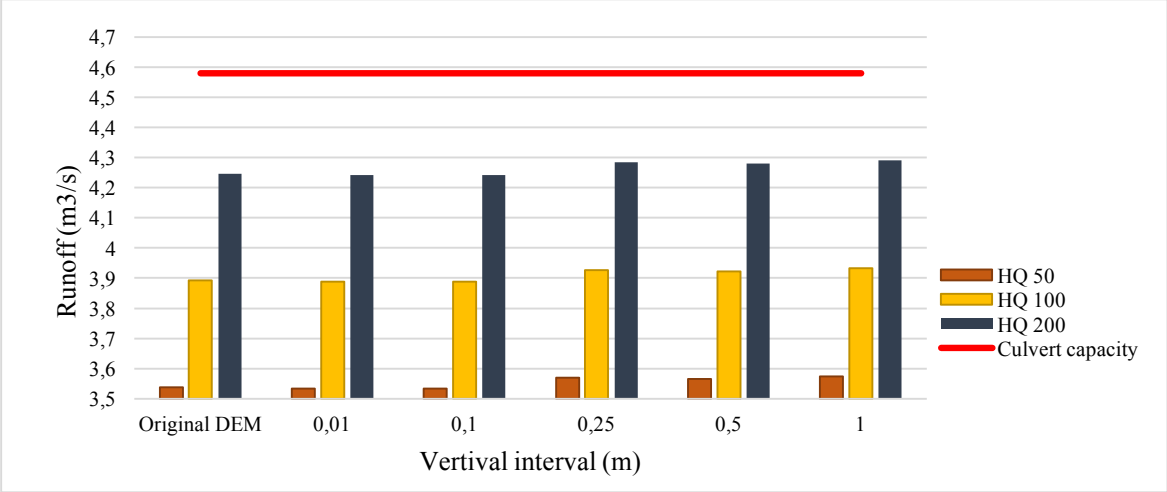

Figure 28. The estimated runoff HQ50, HQ100 and HQ200 to the main culvert based on the modelled watersheds derived by the the TFM model. The maximum capacity of the culvert is presented by the red line.

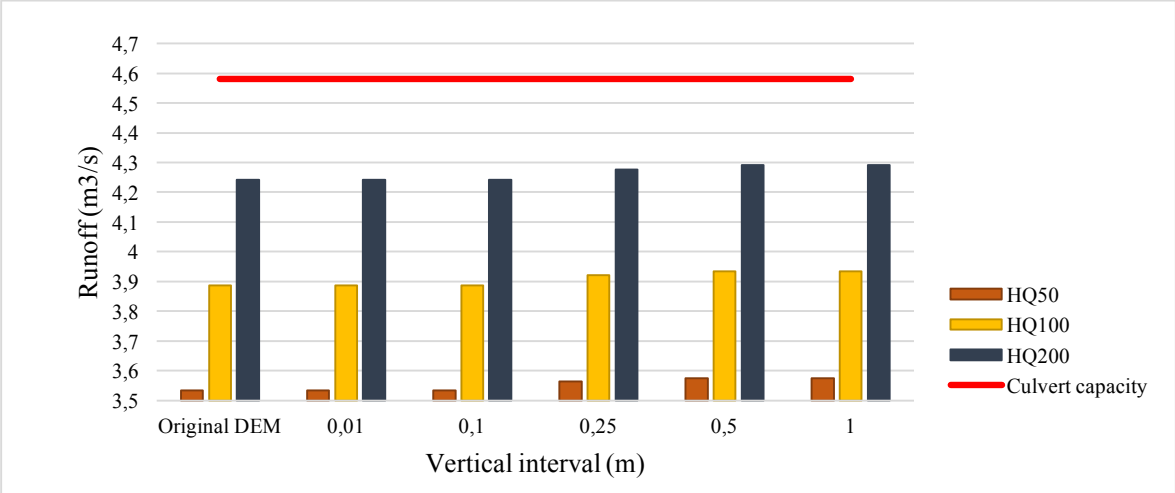

Figure 29. The estimated runoff HQ50, HQ100 and HQ200 to the main culvert based on the modelled watersheds derived by the the D8 model. The maximum capacity of the culvert is presented by the red line.

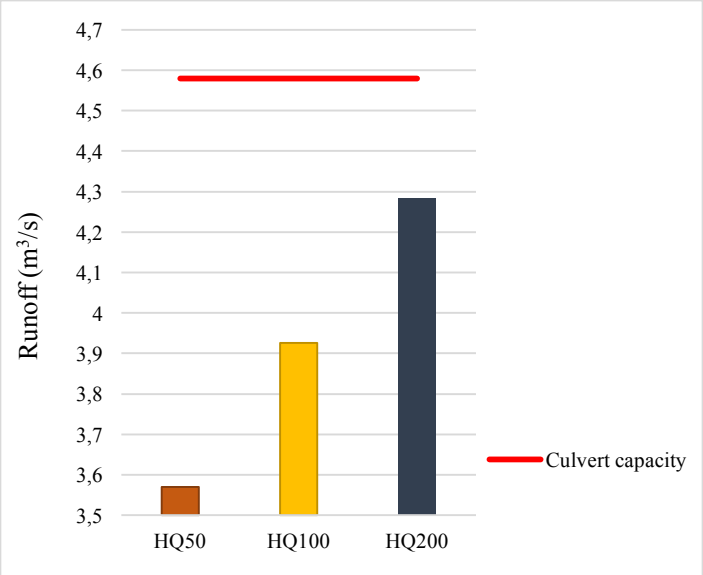

Figure 30. The estimated runoff HQ50, HQ100 and HQ200 to the main culvert based on the manually measured watershed. The maximum capacity of the culvert is presented by the red line.

According to the calculated HQ50, HQ100 and HQ200, based on the sizes of modelled watersheds (figure 28 and 29) and the manually delineated watershed (figure 30), the threshold for the culvert was not exceeded.

5. Discussion

The consequences of climate changes will affect all sectors of society. Setbacks will be faced not only for the ecosystems, but for the natural and cultural environment as well (MSB, 2010). Moreover, are changes in the precipitation patterns in Sweden expected, such as increased events of intense short-duration rainfall and higher intensities of day long-duration rainfall. Water accumulating in depressions, due to the lack of capacity of the drainage system, causes flooded and impassable roads. By tracking the contributing drainage area to depressions using elevation data, runoff to a certain point in the landscape can be estimated. Based on the sizes of the modelled and manually delineated watersheds in this study, runoff for 50-, 100- and a 200year return periods was calculated to a single culvert. According to the estimated flows, using the maximum capacity of the culvert as a threshold, the risk of a potential flood is not likely.

The manually measured watershed show prominent differences in shape and size when compared to the modelled catchments. In general, the models would produce smaller catchments than the manually delineated watershed, and most of the modelled cells are within its external boarder (table 3). When comparing the outlines of the manually measured watershed to the original DEM, it is evident it deviates from the ridgelines (figure S3, see appendix 3). In fact, the manually delineated catchment is enclosing part of the topographic peaks in the area. With this in mind, it is important to reconsider the level of accuracy of the manually measured watershed. Modelling catchments with vertical interval of 0,25m or higher, the north-western part of the measured catchment is enclosed (figure 16, 17 and 18). However, using the DEMs with higher resolution, this will not be the case (figure 13, 14 and 15). This suggests that the edge of a ridge line, located in an area where the relief is between 0,1 - 0,25 metre, has levelled out. Based on these uncertainties the manually delineated watershed must be rejected.

The watersheds produced by the two models are similar, and they do not differ significantly concerning size (table 4). In general, the sizes of the catchments would increase with lower vertical interval (figure 20), meaning that the sizes of the watersheds are depending on the input DEM. When increasing the interval along the z-axis, the number of cells stretching beyond the overlapping area are increasing for the D8 catchments (figure 22). For the TFM catchments, the case is reversed, as the number of cells stretching beyond the overlapping area are decreasing when the vertical interval is increased. Deriving watersheds for the additional culverts, using a DEM with 0,05m vertical resolution, the differences between the modelled catchments are no longer minor (figure 27). By inspection, most cells from the D8 catchments are contributing to the overlapping area, and appears as if the TFM catchments are enclosing the D8 catchments and extending them further. This suggests that the TFM model encloses more of D8 catchments vertical interval is low, and the D8 catchments encloses more of the TFM catchments when the interval is high. Though, the additional watersheds are derived using only a single DEM, but it is also an indication that the TFM catchments will enclose a larger number of D8 cells when the vertical resolution is high, as suggested.

Since the TFM model can divert the flow in multiple directions, a single cell can contribute

with water to various watersheds (figure S22, see appendix 6). Therefore, an assumption could be that the TFM catchments would stretch further beyond the overlapping catchment area than the D8 catchments, for all the DEMs tested. When the vertical interval increases, the flat areas are extending, and models use different methods to treat these surfaces. The D8 algorithm will use the adjacent cells to estimate the flow direction of a flat cell. Thus, cells within a flat area can be assigned different directions, routing the flow in detours before finding the cell with lowest elevation representing the 'true outlet'. As the TFM model will identify the outlet before assigning a flat cells and artificial slope, the flow will be routed straight through the flat surface. Modelling surfaces using a DEM with increased vertical interval, D8 cells extending from the overlapping area is a possible consequence, thus yielding unlikely flow directions, of the flat surfaces. However, the D8 algorithm also would account for cells in areas consisting of 'mixed' concave and flat surfaces, beyond the overlapping area, that the TFM algorithm would not. In these areas, the D8 model continues routing the flow 'out' of the catchment, extending its size by making a detour before entering the watershed again. The rejection of the manually delineated watershed makes it difficult to determine which of the models provided the most accurate result compared to 'real life'. In an assessment carried out by Pilesjö & Hasan (2014) nine flow routing models was tested on mathematical surfaces representing concave, convex, plane and saddle landforms. The accuracy of the models was determined by comparing their significant differences and their spatial distribution of error on the surfaces. Among the tested algorithms, the D8 yielded the poorest results. The TFM model would not provide the best results for all surfaces, but the most accurate results in total.

Addressing the subject of flat areas further, both models faced problems reaching the location of the culvert. The culvert is situated in an area where the slope gradients between the cell is rather small, differing by only millimetres. Preparing the DEMs using the fill operators will create a raised plane surface, of about 0.02 km^2, above the culvert. To elude this issue, new pour points was placed above the area in a cell corresponding to the accumulated flow (Appendix 5). A raw DEM will always include artefacts, and it requires sink removal to enhance the flow. Eliminating artefacts by filling depressions will simultaneously impact the topographic characteristics of the DEM. Despite the known consequences, adapting the DEM with a fill operator is the most common way to prepare DEMs. Alternative methods have been presented, such as breaching through depressions by lowering the neighbouring cells, or 'stream burning' by lowering the elevation of stream lines through ancillary data (Lindsey & Duhn, 2015). Removing depression through a fill operator brought a somewhat unsatisfying result for this study, and an alternative approach could possibly have enhanced the results. Though, choosing a fill operator in this case appeared more convenient, as the vertical modification of the DEMs increased the flat surfaces to begin with.

Watershed runoff is due to multiple factors and is not fully dependent on the size of the catchments. Modelling the runoff based on elevation data exclusively is a somewhat limited approach, as it does not consider factors such as the composite of the surface material, infiltration nor underground flow directions. Deriving catchments without using ancillary data therefore yield uncertainties of the water flow, which should be acknowledged when suggesting that the culvert in this study is not undersized.

6. Conclusions

The deviations between watersheds yield by the D8 and the TFM algorithm were minor concerning size, shape and location. The differences depended to a large extent on the DEM used as input, as both size and shape of the modelled catchments alter when the vertical interval increases. However, the number of cells stretching beyond the common area differ between the models depending on the extent of flat surfaces in the DEM. Based on the 6 DEMs with varying vertical intervals tested in this study, the TFM catchments stretches further beyond the overlapping area than the D8 catchments when the vertical resolution is high. In contrary to the TFM model, the D8 catchments exceeds the common area further when the vertical resolution is low. Comparing the modelled catchments to the manually delineated watershed, the watersheds does not always deviate in size but in shape, without exception. Modifying vertical resolution of the DEMs increases the extent of flat areas, and low ridges are levelled out. The modelled catchments and the manually measured watershed only resemble one another when using DEMs with large vertical intervals, concluding that delineating a watershed manually has disadvantages, as low topographic ridges in the landscape are easily misjudged.

Based on the sizes of the watersheds in this study, the estimated runoff 50-, 100- and 200year return period, suggests that culvert investigated is not in risk of a potential flood.

7. References

Aguilar, F. J., J. Mills, J. Delgado, M. Aguilar, J.G. Negreiros and J. L. Pérez. 2010. *Modelling vertical error in LiDAR-derived digital elevation models*. ISPRS Journal of Photogrammetry and Remote Sensing 65 (2010) 103–110

ArcGIS. 2012. Sverige länsgränser. Retrieved April 22 2017 from http://www.arcgis.com/home/item.html?id=912b806e3b864b5f83596575a2f7cb01

ArcGISpro. 2017. How Watershed Work. Retrieved Mars 29 2017 form http://pro.arcgis.com/en/pro-app/tool-reference/spatial-analyst/how-watershed-works.htm

Bater, C. W. and N. Coops. 2009. *Evaluating error associated with lidar-derived DEM interpolation.* Integrated Remote Sensing Studio, Department of Forest Resources Management, University of British Columbia. Canada: Vancouver. Computers & Geosciences 35 (2009) 289–300. doi:10.1016/j.cageo.2008.09.001

Christensen, J. H. and O. B. Christensen. 2003. *Climate modelling: Severe summertime flooding in Europe.* Nature 421, 805-806. doi:10.1038/421805a

Burges, S. and M. Costa-Cabral. 1994. *Digital elevation model networks (DEMON)): A model of flow over hillslopes for computation of contributing and dispersal areas.* Water resources research, vol. 30. No. 6. Pages 1681-1692.

Environmental Protection Agency (EPA). 1993. *Handbook: Urban runoff pollution Prevention and Controll Planing.* EPA/625/R-93/004. Office of research and Development. USA: Ohio

Environmental System Research Institute (ESRI). 2011. *Fill.* Retrieved May 23 2017 from http://webhelp.esri.com/arcgisdesktop/9.3/index.cfm?TopicName=fill

Environmental System Research Institute (ESRI). 2012a. *Determining flow direction*. Retrieved Mars 29 2017 from http://webhelp.esri.com/arcgisdesktop/9.3/index.cfm?TopicName=Determining_flow_direction

Environmental System Research Institute (ESRI). 2012b. *Calculating flow direction*. Retrieved Mars 29 2017 from http://webhelp.esri.com/arcgisdesktop/9.3/index.cfm?TopicName=Calculating_flow_accumulation

Environmental System Research Institute (ESRI). 2016. *Flow Accumulation*. Retrieved Mars 29 2017 from http://desktop.arcgis.com/en/arcmap/10.3/tools/spatial-analyst-toolbox/flow-accumulation.htm

Europaparlamentets och rådets direktiv. 2007. *Bedömning och hantering av översvämningsrisker 2007/60/EG.* Europeiska unionens officiella tidning 2007, 288/27.

Garbrecht, J., L. Martz. 1996. The assignment of drainage direction over flat surfaces in raster digital elevation models. Journal of Hydrology 193 (1997) 204-213

Gyasi-Agyei, Y., G. Willgoose, and F. De Troch. 1995. Effects of vertical resolution and map scale of digital elevation models on geomorphological parameters used in hydrology. Hydrological Processes, Volume 9, Issue 3-4. DOI: 10.1002/hyp.3360090310

Hasan, A., P. Pilesjö and A. Persson. 2012. *Drainage Area Estimation in Practice, how to tackle artefacts in real world data* in *the proceeding Surface models for geosciences.* Symposium GIS Ostrava 2012 Ostrava, Czech republic.

Allen, S. K., J. Boschung, V. Bex, P. M. Midgley, A. Nauels, G. K. Platter, T. F Stocker, M. M. B. Tignor. Et al. 2013. *Climate Change 2013: The Physical Science Basis*. Contribution of Working Group I to the Fifth Assessment Report of the Intergovernmental Panel on Climate Change (IPCC). USA: New York

Merwade, V and Saksena, S. 2015. *Incorporating the effect of DEM resolution and accuracy for improved flood inundation mapping*. Journal of Hydrology 530 (2015) 180–194

Meyer, L. A. and R. K. Pachauri. 2014. *Climate Change 2014: Synthesis Report*. Contribution of Working Groups I, II and III to the Fifth Assessment Report of the Intergovernmental Panel on Climate Change (IPCC) Switzerland: Geneva

Barros, D. J., T. E. Bilir, M. Chatterjee, V. R. Dokken, K. L. Ebi, Y. O. Estrada, C. B Field, K. J. Mach et al. 2014. Climate Change 2014: *Impacts, Adaptation, and Vulnerability Part A.* Contribution of Working Group II to the Fifth Assessment Report of the Intergovernmental Panel on Climate (IPCC). USA: New York

Domingue, J. O. and S. K, Jenson. 1988. *Extracting topographic structure from digital elevation data for geographic information system analysis.* Photogrammetric engineering and remote sensing, 54(11), 1593-1600.

Li, J. and D. Wong. 2010. Effects of DEM sources on hydrologic applications. Computers, Environment and Urban Systems 34 (2010) 251–261. doi:10.1016/j.compenvurbsys.2009.11.002

Klimatanpassningsportalen. 2016. *Vägar och järnvägar.* Retrieved April 21 2017 from http://www.klimatanpassning.se/hur-paverkas-samhallet/kommunikationer/vagar-och-jarnvagar-1.107430

Kumar, M., R. Kumar, P. K. Singh, M. Singh, K. K. Yadav and H. K. Mittal. 2015. *Catchment*

delineation and morphometric analysis using geographical information system. Water Science & Technology 72.7 2015

Lantmäteriet. 2016a. *GSD-Höjddata, grid 2+*. Retrieved February 19 2017 from https://www.lantmateriet.se/sv/Kartor-och-geografisk-information/Hojddata/GSD-Hojddata-grid-2/

Lantmäteriet. 2016b. Product description: GSD-grid2+. Document version 2.3.

Länsstyrelsen. 2017. Vederslöv. Sockencentrum, bebyggelsemiljö. Kulturmiljö av länsintresse. Retrieved from http://www.lansstyrelsen.se/Kronoberg/Sv/samhallsplanering-och-kulturmiljo/kulturmiljoprogram/vaxjo/Pages/vederslov.aspx

Lindsay, J. 2015. *Efficient hybrid breaching-filling sink removal methods for flow path enforcement in digital elevation models.* Hydrological Processes, 30(6), 846-857. http://dx.doi.org/10.1002/hyp.10648

Lindsay, J., K. Dhun. 2015. *Modelling surface drainage patterns in altered landscapes using LiDAR*. International Journal of Geographical Information Science, 29(3), 397-411. http://dx.doi.org/10.1080/13658816.2014.975715

Meidment, D. 2002. *Arc Hydro: GIS for Water resources. Vol 1*. ESRI. USA: California

Moore I. D., R. B. Grayson and A. R. Ladson. 1991. Digital terrain modelling: a review of hydrological, geomorphological, and biological application. *Hydrological Processes* 5: 3–30

Myndigheten för samhällsskydd och beredskap (MSB). 2010. Ekonomiska konsekvenser av kraftiga skyfall. Publikationsnummer MSB 0187-10.

O'Callaghan, J. and D. Mark. 1984. The extraction of drainage networks from digital elevation data. *Computer Vision, Graphics, And Image Processing*, 28(3), 323-344. http://dx.doi.org/10.1016/s0734-189x(84)80011-0

Olsson, J. and K. Foster. 2013. Extrem korttidsnederbörd i klimatprojektioner för Sverige. *SMHI Klimatologi,* 6.

Olsson, J., B. Armheimer, M. Borris, C. Donnelley, K. Foster, G. Nikulin, M. Persson and A-M. Perttu. 2016. *Hydrological Climate Change Impact Assessment at Small and Large Scales: Key Messages from Recent Progress in Sweden.* Climate 2016, 4(3), 39; doi:10.3390/cli4030039

Pilesjö, P. 2008. *An integrated raster-TIN surface flow algorithm.* Advances in Digital Terrain. Analysis, edited by Q. Zhou, B. Lees, and G. Tang, pp. 237-255, Springer, Berlin.

Pilesjö, P., A. Hasan. 2014. *A Triangular Form-based Multiple Flow Algorithm to Estimate Overland Flow Distribution and Accumulation on a Digital Elevation Model.*

Transactions in GIS, 18(1), 108-124. http://dx.doi.org/10.1111/tgis.12015

Qin, C., A.-X. Zhu, T. Pei, B., Li, C. Zhou and L. Yang. 2007. *An adaptive approach to selecting a flow-partition exponent for a multiple-flow-direction algorithm*. International Journal of Geographical Information Science, 21(4), 443-458.

Quinn, P., K. Beven, P. Chevallier, and O. Planchon. 1991. *The prediction of hillslope flow paths for distributed hydrological modelling using digital terrain models,* Hydrological Processes 5, 9-79.

Qin, C-Z and L. Zahn. 2012. Parallelizing flow-accumulation calculations on graphics processing units—From iterative DEM preprocessing algorithm to recursive multiple-flow-direction algorithm. Computers & Geosciences 43 (2012) 7–16

Statens plankverks författaransamling. 1980. SBN 1980. Svensk byggnorm. Retrieved from http://www.lansstyrelsen.se/Kronoberg/Sv/samhallsplanering-och-kulturmiljo/kulturmiljoprogram/vaxjo/Pages/vederslov.aspx

Sveriges Riksstad. 2009. Förordning (2009:956) om översvämningsrisker. Svensk författningssamling 2009:956

Sveriges metrologiska och hydrologiska institut (SMHI). 2002. *Avrinningen I Sverige.* Faktablad 12.

Sveriges metrologiska och hydrologiska institut (SMHI). 2007. *Avrinningens variation 1961 – 2005*. Faktablad 36.

Sveriges metrologiska och hydrologiska institut (SMHI). 2012. Huvud-och delavrinningsområden, vattendelare. Retrieved April 22 2017 http://opendata-catalog.smhi.se/explore/

Sveriges metrologiska och hydrologiska institut (SMHI). 2015a. *Avrinningsområde*. Retrieved April 2 2017from http://www.smhi.se/kunskapsbanken/hydrologi/avrinningsomrade-1.6704

Sveriges metrologiska och hydrologiska institut (SMHI). 2015b. *Markavvattning – Så leds vattnet bort.* Retrieved April 2 2017 from http://www.smhi.se/kunskapsbanken/markavvattning-sa-leds-vatten-bort-1.89795

Sveriges metrologiska och hydrologiska institut (SMHI). 2015c. *Återkomsttider.* Retrieved April 2 2017 from http://www.smhi.se/kunskapsbanken/aterkomsttider-1.89085

Sveriges metrologiska och hydrologiska institut (SMHI). 2015d. Framtidsklimatet I Konobergs län – Enligt RCP scenarior. Klimatologi nr 27.

Statens offentliga utredningar. 2007. SOU 2007:60. *Sverige inför klimatförändringarna-hot och möjligheter*. Stockholm: Miljö- och energidepartementet.

Svenskt Vatten. 2016. *Avledning av dag-, drän- och spillvatten, Funktionskrav, hydrauliks dimensionering och utformning av allmänna avloppssystem*. Del I – Policy och funktionskrav för samhällens avvattning. Publikation 110.

Tarboton, D. G. 1997. *A new method for the determination of flow directions and upslope areas in grid digital elevation models.* Water Resources Research, 32(2), 309-319.

Trafikverket. 2014. *Trummor - Naturens väg under vägar och järnvägar*. Retrieved Mars 26 2017 from http://online4.ineko.se/trafikverket/Product/Detail/43100

Trafikverket. 2016a. *Underhåll av väg och järnväg*. Retrieved Mars 26 2017 from http://www.trafikverket.se/resa-och-trafik/underhall-av-vag-och-jarnvag/

Trafikverket. 2016b. *Handlingsplan för Trafikverkets klimatanpassningsstrategi.* Version 1.0. Trafikverket, Borlänge

United States Department of Agriculture (USDA). 2017. *Reading topographic maps.* Retrieved 22 May 2017 from https://www.nrcs.usda.gov/wps/portal/nrcs/detail/nh/technical/dma/?cid=nrcs144p2_015706

Vägverket. 2008. *VVMB 310 Hydraulisk dimensionering. 2008:61*. Vägverkets tryckeri, Borlänge.

Wilson, John P. 2012. Digital terrain modeling. Geomorphology 137 (2012) 107–121. doi:10.1016/j.geomorph.2011.03.012

Wilson, J. P., G. Aggett, Y. Deng, and C. S. Lam. 2008. *Water in the landscape: A review of contemporary flow routing algorithms in Advances in Digital Terrain Analysis*, Edited by Q. Zhou, B. Lees, and G. Tang, pp. 213-236, Springer, Berlin.

Zhao, G. J., J. F. Gao, P. Tian, Peng and K Tian. 2009. *Comparison of two different methods for determining flow direction in catchment hydrological modeling***.** Water Science and Engineering 2(4): 1-15 doi:10.3882/j.issn.1674-2370.2009.04.001

Appendix 1 – Manually measured watershed to the main culvert in Vederslöv

Figure S1. The manually measured catchment area in Vederslöv. Outlined by Bertil Nordkvist using Fastighetskartan with 5m contour lines.

Appendix 2 – Orto photo covering the catchment areas in Vederslövssjön

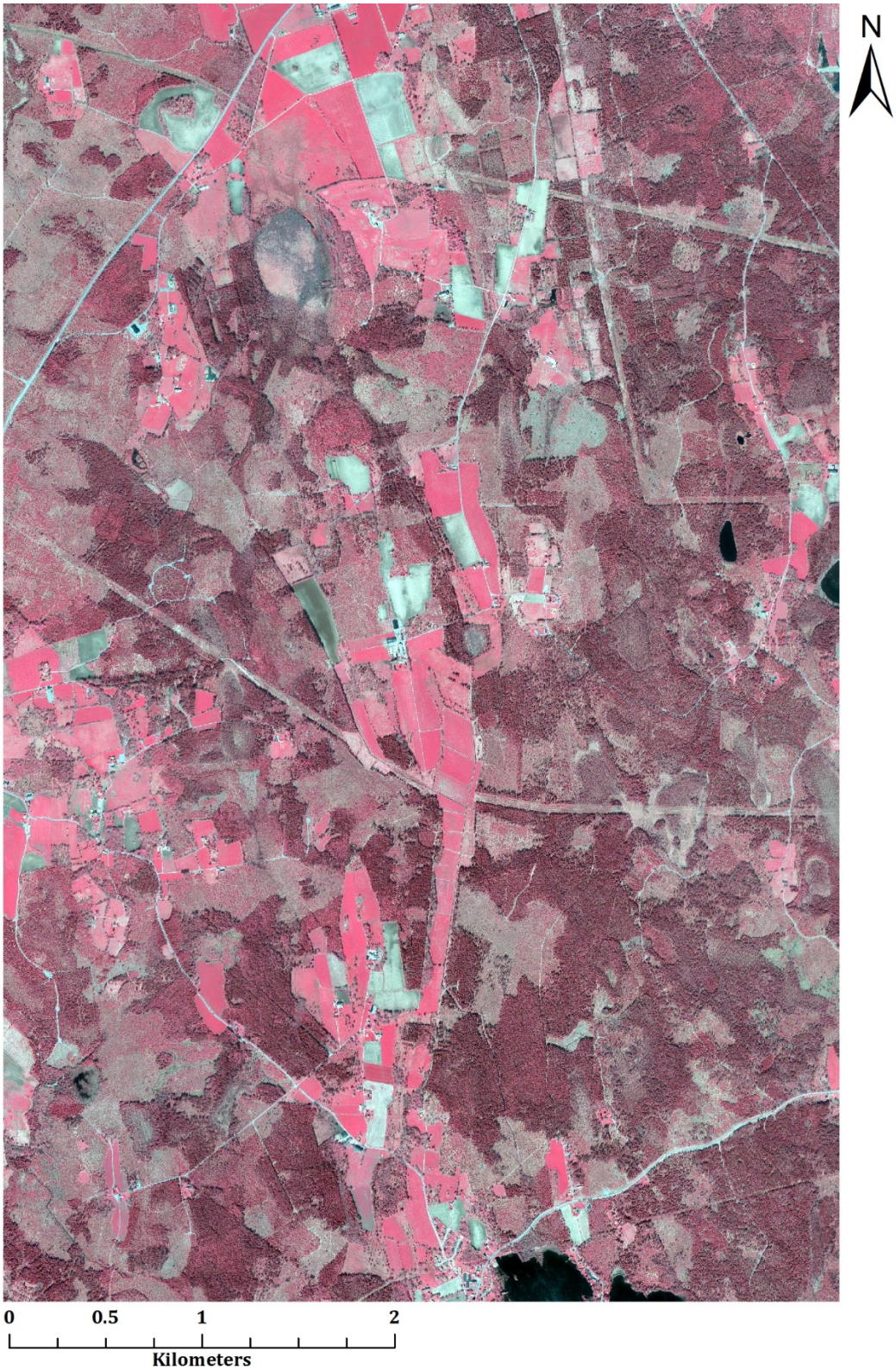

Figure S2. The orto photo, in false colour composite, covering the area above Vederslövssjön.

Appendix 3. The manually delineated catchment compared to the elevation

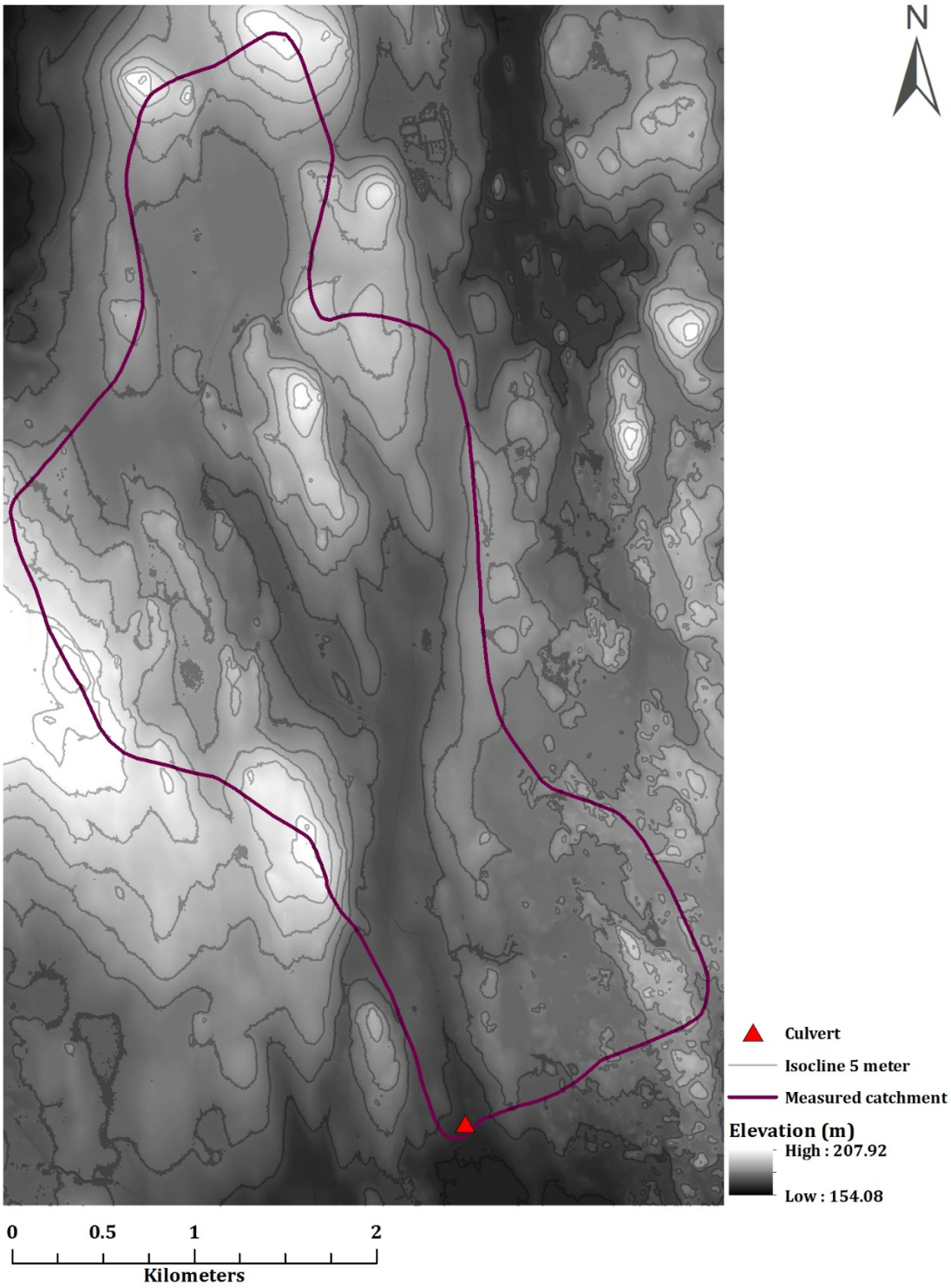

Figure S3. The manually measured catchment to the culvert, placed on top of the original DEM with 0,05m vertical resolution. The elevation differences in the area is enhanced by isoclines curves of 5m.

Appendix 4. DEMs with varying vertical resolution

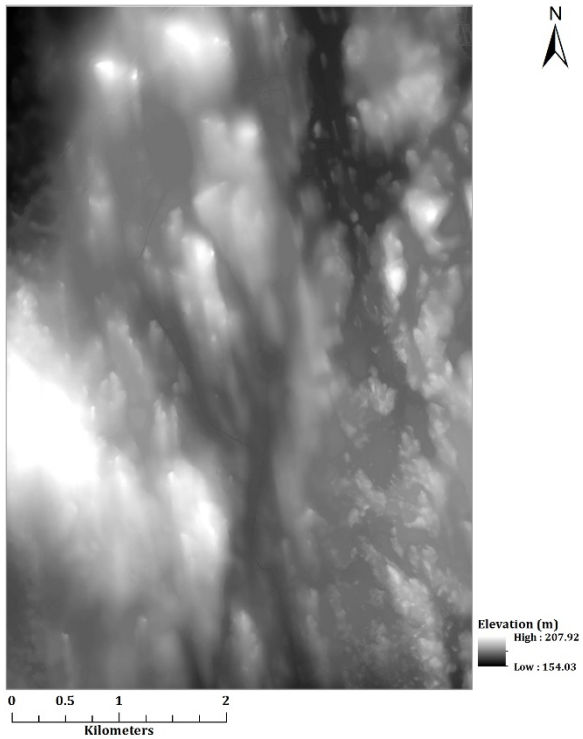

Figure S4. DEM with 0,05m vertical resolution

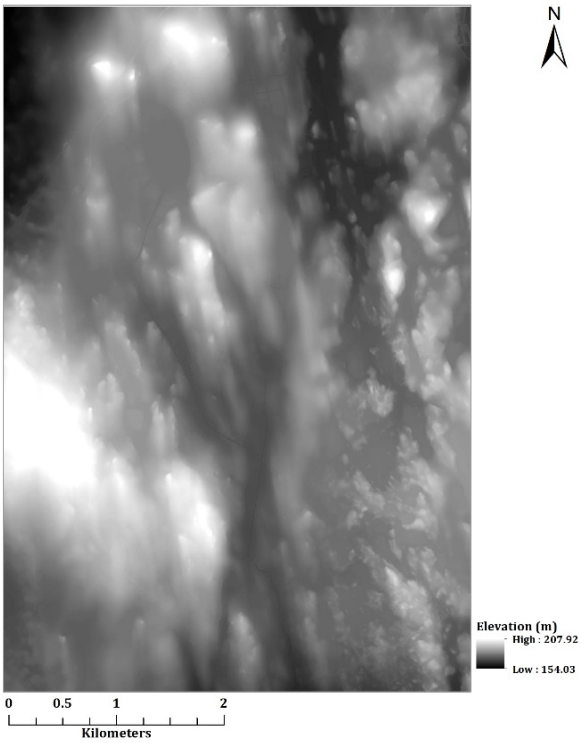

Figure S5. DEM with 0,01m vertical interval

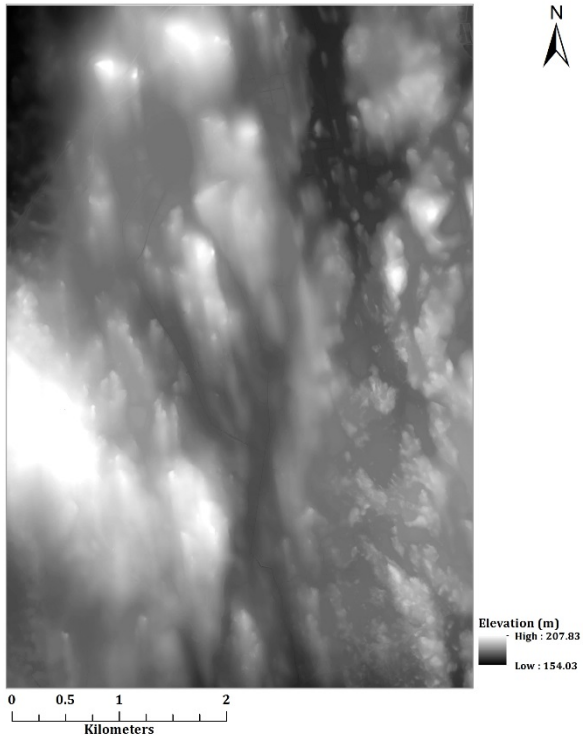

Figure S6. DEM with 0,10m vertical interval

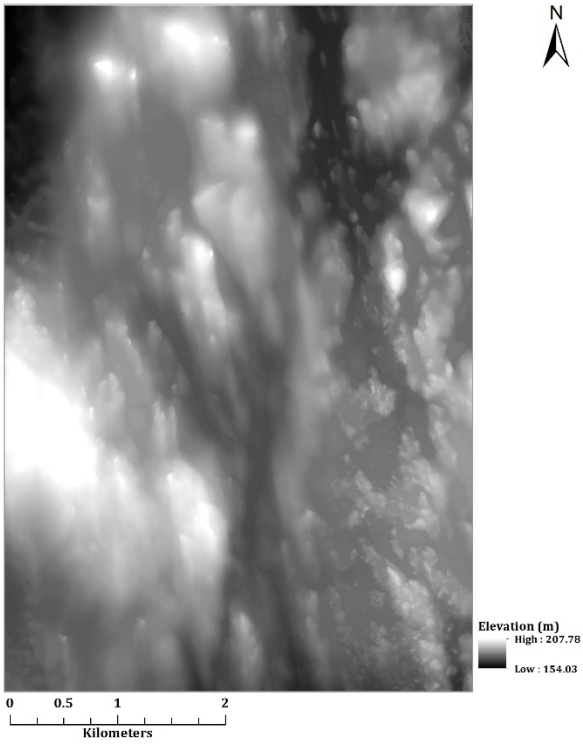

Figure S7. DEM with 0,25m vertical interval

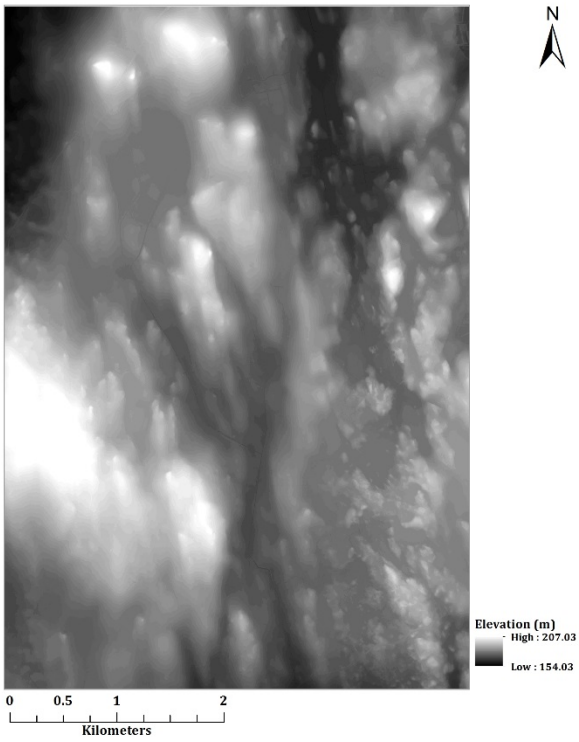

Figure S8. DEM with 0,50m vertical interval

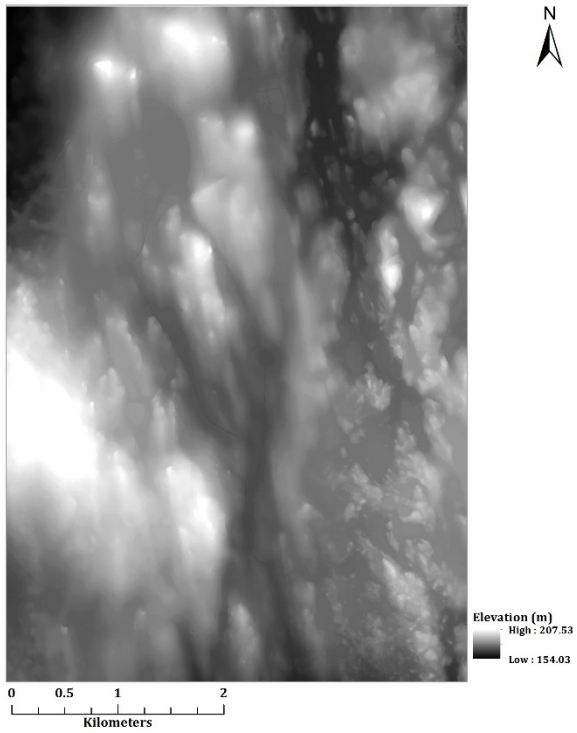

Figure S9. DEM with 1m vertical interval

Appendix 5. Accumulated flow in the culvert area

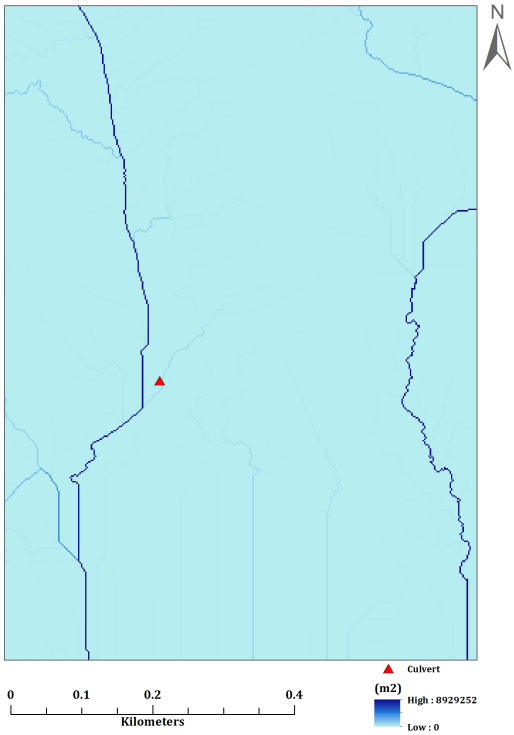

Figure S10. The accumulated flow produced by the D8 algorithm using a DEM with 0,05m vertical resolution

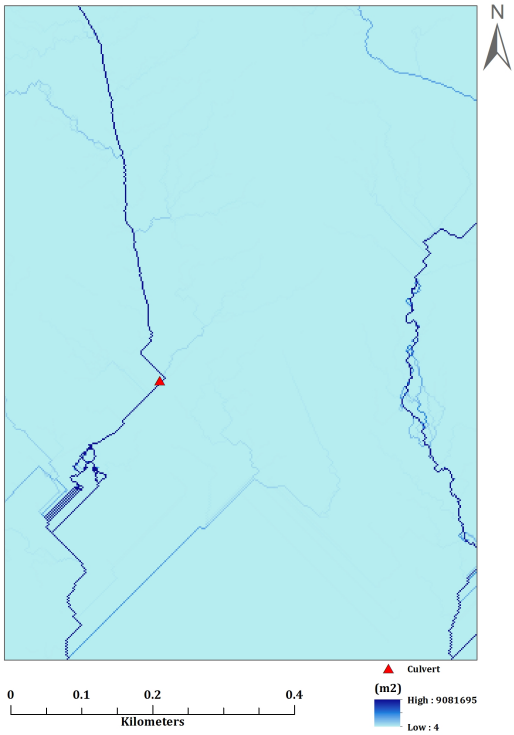

Figure S11. The accumulated flow produced by the TFM algorithm using a DEM with 0,05m vertical resolution

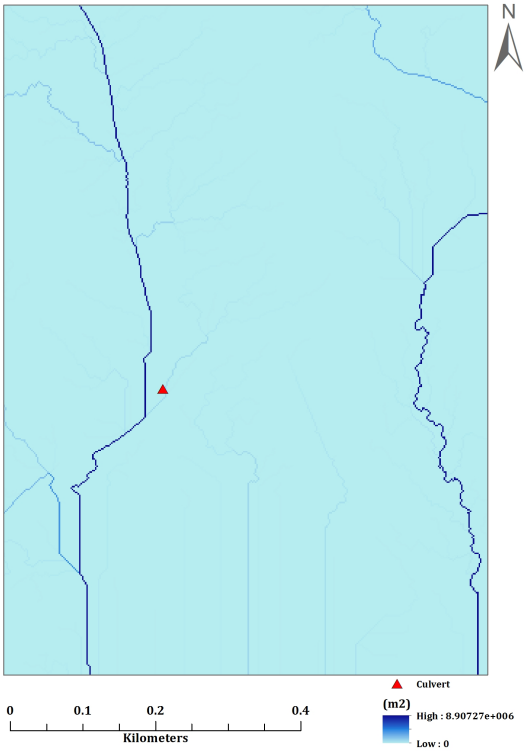

Figure S12. The accumulated flow produced by the D8 algorithm using a DEM with 0,01m vertical interval

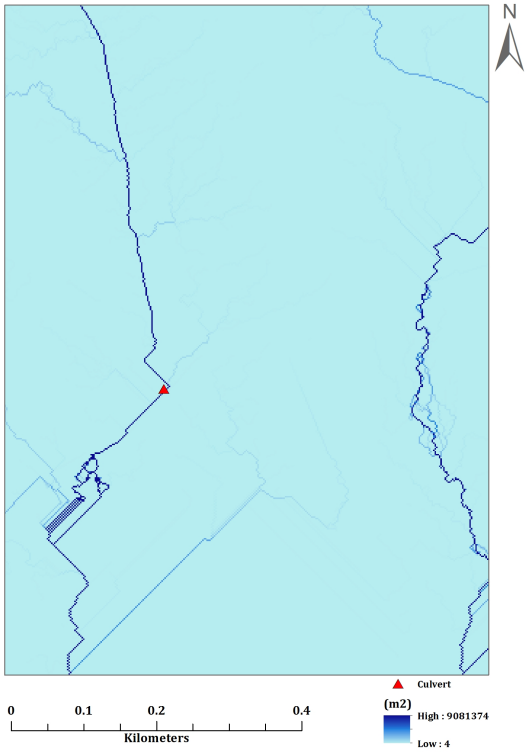

Figure S13. The accumulated flow produced by the D8 algorithm using a DEM with 0,01m vertical interval

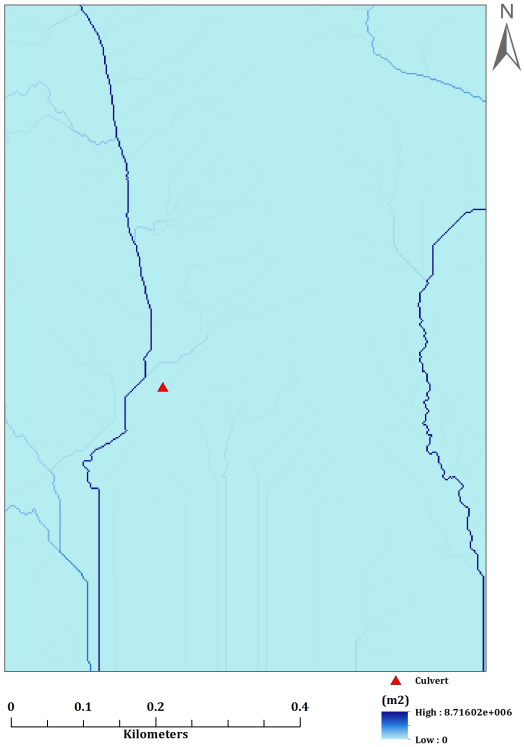

Figure S14. The accumulated flow produced by the D8 algorithm using a DEM with 0,1m vertical interval

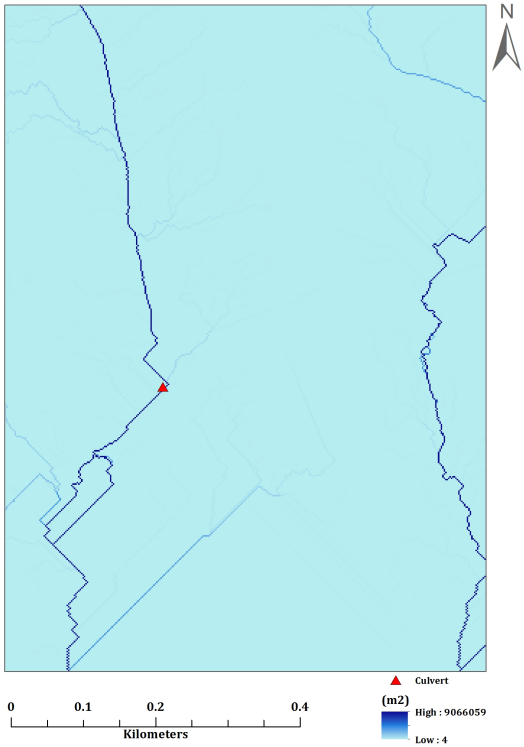

Figure S15. The accumulated flow produced by the TFM algorithm using a DEM with 0,1m vertical interval

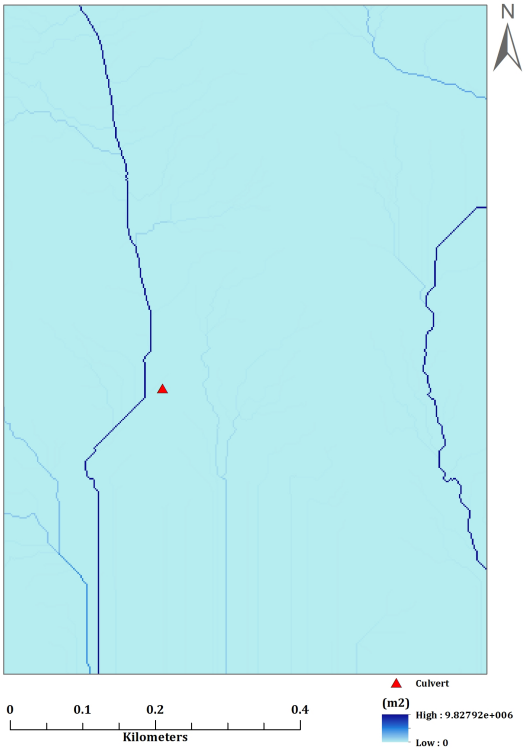

Figure S16. The accumulated flow produced by the D8 algorithm using a DEM with 0,25m vertical interval

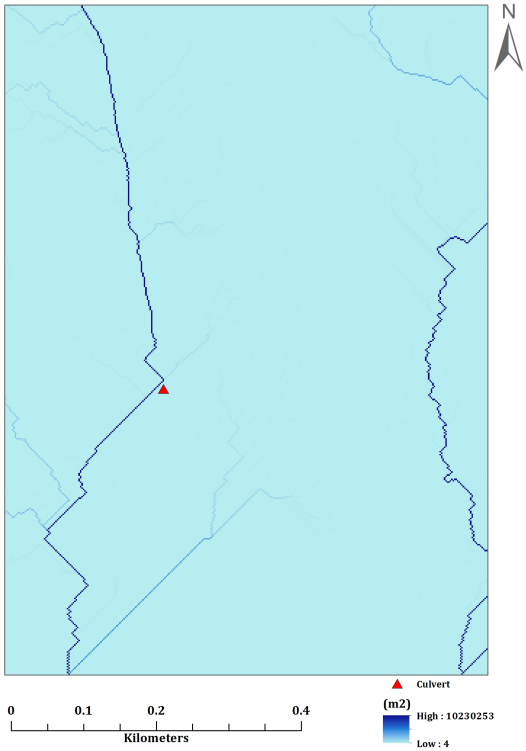

Figure S17. The accumulated flow produced by the TFM algorithm using a DEM with 0,25m vertical interval

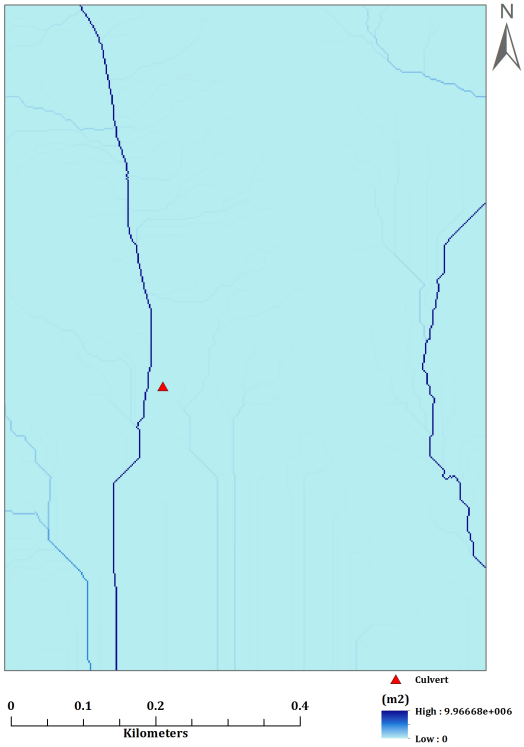

Figure S18. The accumulated flow produced by the D8 algorithm using a DEM with 0,50m vertical interval

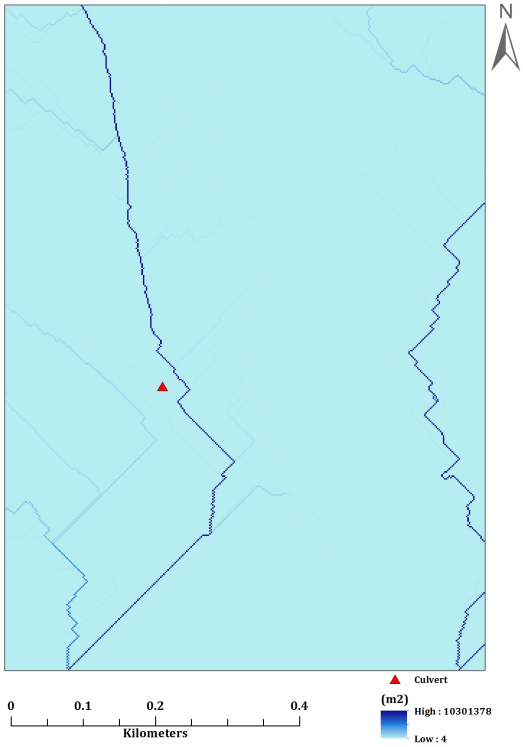

Figure S19. The accumulated flow produced by the TFM algorithm using a DEM with 0,50m vertical interval

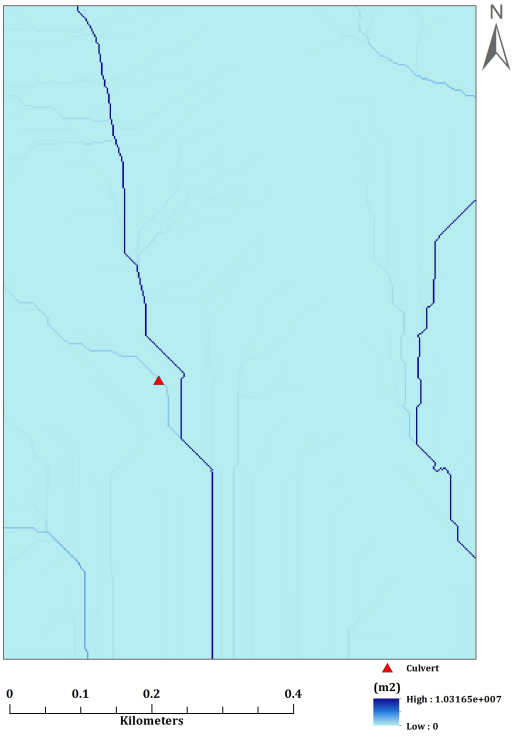

Figure S20. The accumulated flow produced by the D8 algorithm using a DEM with 1m vertical interval

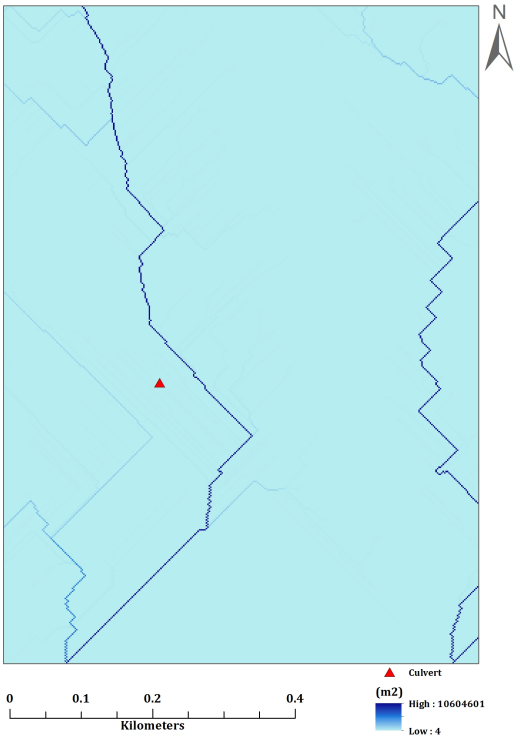

Figure S21. The accumulated flow produced by the TFM algorithm using a DEM with 1m vertical interval

Appendix 6. Watersheds yield by additional culverts merged together with the watershed from the main culvert

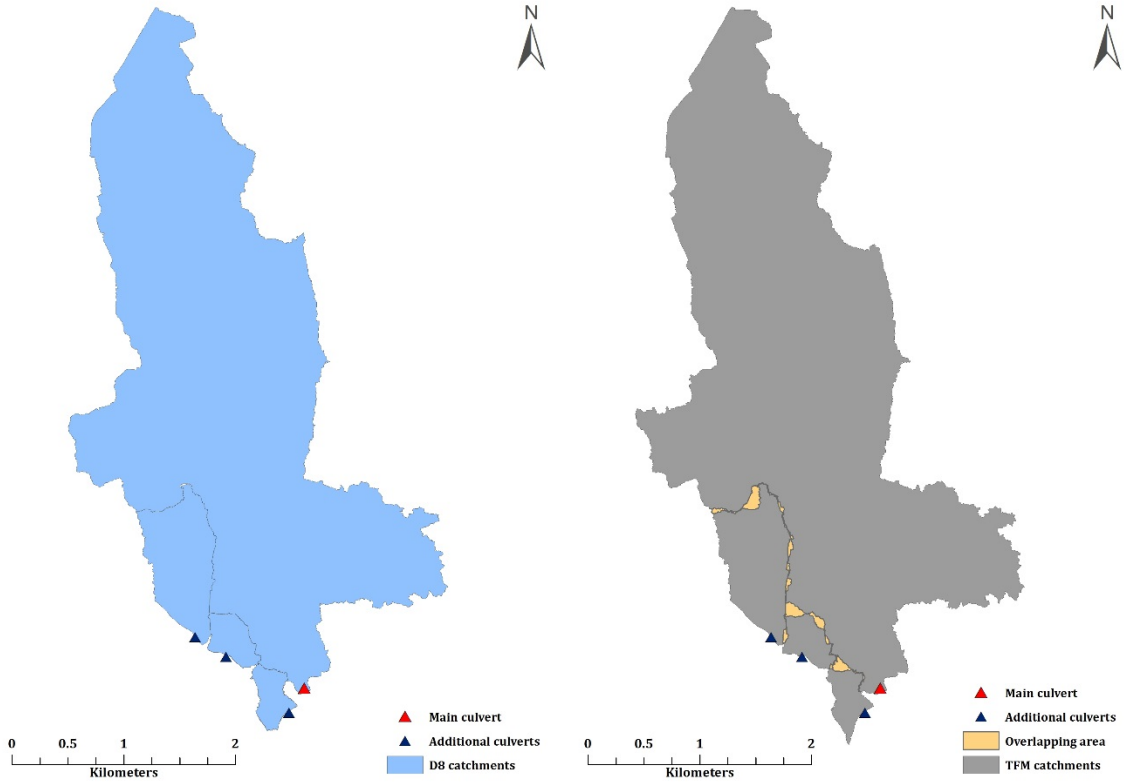

Figure S22. The watersheds from the additional culverts merged together with the watershed to the main culvert. The D8 catchments (left) will partly connect, sharing most of their edges. In contrast to the D8 model, the TFM model generates catchments that will overlap when patched together.

Institutionen för naturgeografi och ekosystemvetenskap, Lunds Universitet.
Studentexamensarbete (seminarieuppsatser). Uppsatserna finns tillgängliga på institutionens geobibliotek, Sölvegatan 12, 223 62 LUND. Serien startade 1985. Hela listan och själva uppsatserna är även tillgängliga på LUP student papers (https://lup.lub.lu.se/student-papers/search/) och via Geobiblioteket (www.geobib.lu.se)

The student thesis reports are available at the Geo-Library, Department of Physical Geography and Ecosystem Science, University of Lund, Sölvegatan 12, S-223 62 Lund, Sweden. Report series started 1985. The complete list and electronic versions are also electronic available at the LUP student papers (https://lup.lub.lu.se/student-papers/search/) and through the Geo-library (www.geobib.lu.se)

400 Sofia Sjögren (2016) Effective methods for prediction and visualization of contaminated soil volumes in 3D with GIS
401 Jayan Wijesingha (2016) Geometric quality assessment of multi-rotor unmanned aerial vehicle-borne remote sensing products for precision agriculture
402 Jenny Ahlstrand (2016) Effects of altered precipitation regimes on bryophyte carbon dynamics in a Peruvian tropical montane cloud forest
403 Peter Markus (2016) Design and development of a prototype mobile geographical information system for real-time collection and storage of traffic accident data
404 Christos Bountzouklis (2016) Monitoring of Santorini (Greece) volcano during post-unrest period (2014-2016) with interferometric time series of Sentinel-1A
405 Gea Hallen (2016) Porous asphalt as a method for reducing urban storm water runoff in Lund, Sweden
406 Marcus Rudolf (2016) Spatiotemporal reconstructions of black carbon, organic matter and heavy metals in coastal records of south-west Sweden
407 Sophie Rudbäck (2016) The spatial growth pattern and directional properties of *Dryas octopetala* on Spitsbergen, Svalbard
408 Julia Schütt (2017) Assessment of forcing mechanisms on net community production and dissolved inorganic carbon dynamics in the Southern Ocean using glider data
409 Abdalla Eltayeb A. Mohamed (2016) Mapping tree canopy cover in the semi-arid Sahel using satellite remote sensing and Google Earth imagery
410 Ying Zhou (2016) The link between secondary organic aerosol and monoterpenes at a boreal forest site
411 Matthew Corney (2016) Preparation and analysis of crowdsourced GPS bicycling data: a study of Skåne, Sweden
412 Louise Hannon Bradshaw (2017) Sweden, forests & wind storms: Developing a model to predict storm damage to forests in Kronoberg county
413 Joel D. White (2017) Shifts within the carbon cycle in response to the absence of keystone herbivore *Ovibos moschatus* in a high arctic mire
414 Kristofer Karlsson (2017) Greenhouse gas flux at a temperate peatland: a comparison of the eddy covariance method and the flux-gradient method
415 Md. Monirul Islam (2017) Tracing mangrove forest dynamics of Bangladesh using historical Landsat data
416 Bos Brendan Bos (2017) The effects of tropical cyclones on the carbon cycle
417 Martynas Cerniauskas (2017) Estimating wildfire-attributed boreal forest burn in Central and Eastern Siberia during summer of 2016
418 Caroline Hall (2017)The mass balance and equilibrium line altitude trends of glaciers in northern Sweden

419 Clara Kjällman (2017) Changing landscapes: Wetlands in the Swedish municipality Helsingborg 1820-2016
420 Raluca Munteanu (2017) The effects of changing temperature and precipitation rates on free-living soil Nematoda in Norway.
421 Neija Maegaard Elvekjær (2017) Assessing Land degradation in global drylands and possible linkages to socio-economic inequality
422 Petra Oberhollenzer, (2017) Reforestation of Alpine Grasslands in South Tyrol: Assessing spatial changes based on LANDSAT data 1986-2016
423 Femke, Pijcke (2017) Change of water surface area in northern Sweden
424 Alexandra Pongracz (2017) Modelling global Gross Primary Production using the correlation between key leaf traits
425 Marie Skogseid (2017) Climate Change in Kenya - A review of literature and evaluation of temperature and precipitation data
426 Ida Pettersson (2017) Ekologisk kompensation och habitatbanker i kommunalt planarbete
427 Denice Adlerklint (2017) Climate Change Adaptation Strategies for Urban Stormwater Management – A comparative study of municipalities in Scania
428 Johanna Andersson (2017) Using geographically weighted regression (GWR) to explore spatial variations in the relationship between public transport accessibility and car use : a case study in Lund and Malmö, Sweden
429 Elisabeth Farrington (2017) Investigating the spatial patterns and climate dependency of Tick-Borne Encephalitis in Sweden
430 David Mårtensson (2017) Modeling habitats for vascular plants using climate factors and scenarios - Decreasing presence probability for red listed plants in Scania
431 Maja Jensen (2017) Hydrology and surface water chemistry in a small forested catchment : which factors influence surface water acidity?
432 Iris Behrens (2017) Watershed delineation for runoff estimations to culverts in the Swedish road network : a comparison between two GIS based hydrological modelling methods and a manually delineated watershed
433 Jenny Hansson (2017) Identifying large-scale land acquisitions and their agro-ecological consequences : a remote sensing based study in Ghana